Molecular Therapy
Oncolytics
Original Article

Bacterial Carriers for Glioblastoma Therapy

Nalini Mehta,[1,3] Johnathan G. Lyon,[1,2,3] Ketki Patil,[1] Nassir Mokarram,[2] Christine Kim,[1] and Ravi V. Bellamkonda[2]

[1]Wallace H. Coulter Department of Biomedical Engineering, Georgia Institute of Technology and Emory School of Medicine, UA Whitaker Building, 313 Ferst Drive, Atlanta, GA 30332, USA; [2]Department of Biomedical Engineering, Pratt School of Engineering, Duke University, 101 Science Drive, Durham, NC 27708-0271, USA

Treatment of aggressive glioblastoma brain tumors is challenging, largely due to diffusion barriers preventing efficient drug dosing to tumors. To overcome these barriers, bacterial carriers that are actively motile and programmed to migrate and localize to tumor zones were designed. These carriers can induce apoptosis via hypoxia-controlled expression of a tumor suppressor protein p53 and a pro-apoptotic drug, Azurin. In a xenograft model of human glioblastoma in rats, bacterial carrier therapy conferred a significant survival benefit with 19% overall long-term survival of >100 days in treated animals relative to a median survival of 26 days in control untreated animals. Histological and proteomic analyses were performed to elucidate the safety and efficacy of these carriers, showing an absence of systemic toxicity and a restored neural environment in treated responders. In the treated non-responders, proteomic analysis revealed competing mechanisms of pro-apoptotic and drug-resistant activity. This bacterial carrier opens a versatile avenue to overcome diffusion barriers in glioblastoma by virtue of its active motility in extracellular space and can lead to tailored therapies via tumor-specific expression of tumoricidal proteins.

INTRODUCTION

The diffuse and infiltrative nature of glioblastoma (GBM) tumors presents unique challenges for effective treatment. Although surgical resection, radiation, and systemic chemotherapy are the clinical standards of care, the median survival of patients is less than 15 months primarily due to tumor recurrence.[1] Systemic delivery of chemotherapeutics is not effective due to the diffusion barriers imposed by the solid tumor,[2,3] which results in a suboptimal therapeutic concentration of the cancer drug within the tumor. The dominant strategy to overcome diffusion barriers is convection enhanced delivery (CED) whereby a pressure gradient enhances interstitial infusion of drugs.[4] Not only is it challenging to accurately model drug dosing with this method given brain tissue heterogeneity,[5,6] but also the increased pressure within the brain caused by CED could lead to cerebral edema, hemiparesis, and other neurological damage.[7] Therefore, there is a critical need to explore alternate approaches to overcome diffusion barriers that impede adequate drug dosing into solid tumors.

Engineered nanoparticles have been shown to selectively detect and destroy tumor cells.[8–10] Although promising, nanoparticle therapy is still limited by physiological obstacles such as protein adsorption, phagocytic sequestration, renal clearance, as well as physical obstacles such as diffusion, flow, and shear forces, which limit diffusion of nanoparticles to or within tumors.[11–15] In fact, a comprehensive analysis of data from 10 years has indicated that only 0.7% (median) of the administered dose of nanoparticles reach solid tumors.[16] In this study, we report the design of a bacterial carrier, an avirulent strain of Salmonella *typhimurium*, with active motility in extracellular space and within brain tumors, and the capability of expressing apoptotic proteins within the tumor.

The bacterial carrier has mutation in the *msbB* gene that is required for terminal myristoylation of lipid A, a component of the outer membrane in Gram-negative bacteria such as enteropathogenic *Escherichia coli* and *S. typhimurium*.[17] Lipid A is necessary for tumor necrosis factor alpha (TNF-α)-mediated septic shock during food poisoning caused by these bacteria.[18,19] A mutation in *msbB* gene impedes systemic toxicity as evident from in vivo evaluation of this strain in mice.[20,21] This strain has also been used in clinical trials in patients with metastatic melanoma.[22] However, in these clinical trials, no antitumor effect was observed at a maximum patient-tolerated dose of 3×10^8 cfu/m^2 given intravenously. Therefore, although safe, the mere presence of the bacterial strain is insufficient to elicit a tumoricidal response.

Tumor-specific localization of this strain is enabled by a mutation in the *purI* gene (encodes for purine biosynthetic enzyme), which makes the strain deficient in synthesizing purines, creating a need for external sources of purines for its survival and multiplication.[23,24] Tumors are a rich source of purines with adenosine triphosphate concentrations in the range of hundreds of micromolar, whereas healthy tissue concentrations are below detectable levels.[25–27] Thus, given the combination of purine deficiency in the carriers and relative purine abundance in tumors, the carrier exhibits a tumor-seeking propensity.

The bacterial carrier was designed to express wild-type tumor suppressor protein p53, a multifaceted protein that exerts its apoptotic activity through a cooperative effect of transcription-dependent

Received 16 August 2016; accepted 4 December 2016;
http://dx.doi.org/10.1016/j.omto.2016.12.003.

[3]These authors contributed equally to this work.

Correspondence: Ravi V. Bellamkonda, Department of Biomedical Engineering, Pratt School of Engineering, Duke University, 101 Science Drive, Durham, NC 27708-0271, USA.
E-mail: ravi@duke.edu

and transcription-independent pathways.[28–32] In the transcription-dependent pathway, phosphorylated p53 transcriptionally up-regulates a number of pathways that express pro-apoptotic proteins such as BAX, PUMA, NOX, and suppresses anti-apoptotic proteins such as BCL2 and $BCLX_L$. The pro-apoptotic proteins induce permeabilization of outer mitochondrial membrane (OMM) enabling the release of cytochrome *c* (CYCS) and other apoptotic proteins leading to apoptosis. In the transcription-independent pathway, p53 directly activates BAX, which undergoes a conformational switch, oligomerizes, and inserts into OMM leading to apoptosis.[33,34] The significance of p53 in cancer is evident from the fact that more than 50% of cancers with poor clinical prognosis are associated with mutations in the p53 core DNA-binding domain.[35–37] In patients with primary and secondary GBM, the incidence of p53 mutations is 28% and 65%, respectively.[38,39] Several treatment strategies have tried to reactivate the mutated p53, to reconstitute wild-type p53, or to inhibit MDM2 (protein that down-regulates p53).[40–42] However, absence of an efficient delivery system into solid tumors has dwarfed the effectiveness of these therapies.

To enhance the apoptotic activity of the carrier as well as to increase the stability of wild-type p53, bacterial carrier that additionally expresses Azurin was designed. Azurin is a multifunctional protein that induces apoptosis of cancerous cells, inhibits receptor tyrosine kinase-mediated cell signaling and angiogenesis, and is a promising tumoricidal protein.[43–45] Azurin stabilizes p53 by forming a complex and protecting it from undergoing ubiquitination and proteasomal degradation.[46,47] This is important, as the intracellular half-life of p53 is approximately 25–30 min if left unprotected.[46–48] Although full-length Azurin is a potent tumoricidal protein, it does not penetrate GBM cells, nor does it cross the blood-brain barrier in mice when injected intraperitoneally with the pure protein.[49,50] Additionally Azurin is not cytotoxic to non-cancerous healthy cells. A small synthetic peptide (p28) derived from full-length Azurin sequence has been used in phase I clinical trials;[51] however, the p28 peptide does not possess the inhibitory potential of full-length Azurin because there are other non-overlapping domains (p26) within the protein that confer anti-cancer activity specifically targeting tyrosine kinases.[43,50]

Finally, to constrain expression of these tumoricidal proteins to the tumor region, both p53 and Azurin expression by the carriers was engineered to be driven by a hypoxic promoter *pflE*.[52] This approach exploits the hypoxic tumor microenvironment combined with purine-dependent motile carrier to achieve tumor-targeted expression of p53 and full-length Azurin to induce apoptosis of glioblastoma cells (Figure 1A).

RESULTS

Expression of Azurin and p53 from Hypoxia-Inducible *pflE* Promoter Occurs Abundantly under Anaerobic Conditions

The postulated mechanism by which p53- and Azurin-expressing carriers induce apoptosis within tumors is depicted in Figure 1A. Restricted expression of apoptotic proteins Azurin and p53 by hypoxia-inducible *pflE* promoter in *S. typhimurium* strain VNP 20009 (carrier) was attained using specific primers (Table S1). Prior to animal studies, in vitro expression of p53 was confirmed using western blotting after growing the carrier under aerobic and anaerobic conditions (BD Anaerobic GasPak EZ system) (Figure 1B). p53 expression was also confirmed by an ELISA (Figure 1C). *pflE* promoter is not completely shut down under aerobic conditions; therefore, minimal p53 expression was observed under aerobic conditions.[52,53] The expression of Azurin was confirmed using mass spectrometry (Table S2).

Injection of Carriers with Combined Action of Azurin and p53 Suppressed Tumor Growth and Led to Increased Survival

The timeline of carrier injection following tumor implantation is shown in Figure 2A. Carriers capable of expressing both p53 and Azurin were injected intracranially at the tumor implant site to a depth of 1.5 mm using a stereotax on days 7 and 14 post-tumor implant. Overall survival was 19% in treated rats, and 0% in control rats (Figure 2B). Compiled Kaplan-Meier curves over six different animal experiments showed significant difference in survival using a log-rank Mantel-Cox test ($p < 0.0046$), although only a 3-day difference was observed in median survival between control (26 days, $n = 36$) and treated (29 days, $n = 36$) rats.

Tumor volume was assessed by MRI for 12 control and 12 treated rats from two distinct experimental cohorts that had sufficient number of responders for further analysis. An exponential increase in tumor volume was observed for all 12 control rats, whereas 6 (responders) out of 12 treated rats demonstrated tumor suppression (Figure 2C) corresponding with overall survival. MRI brain scans of treated responder rats that were injected in the left cortex with *both* Azurin- and p53-expressing carrier showed dramatic tumor regression following carrier injection compared to control and treated non-responder rats (Figures 2B and 2D). No tumor was readily discriminable by MRI measurement for treated responder rats after 40 days. Another set of studies with rats that were treated singly with carrier expressing either p53 or Azurin (but not both) showed increased tumor growth with no survival (Figures S1A–S1D).

Fluorescent in Situ Hybridization Demonstrates Carrier Migration and Colonization into Deep Tumors

To follow the migration of the intracranially injected carrier, a *Salmonella*-specific, fluorescently labeled 23S rDNA probe was used (Table S1).

In the treated responder rats where the tumor growth was suppressed, negligible number of carriers were observed within the brain and the liver after 100 days post-tumor implant. However, a few carriers were observed in the spleen, indicating that, in the absence of a tumor, carriers have a greater tendency to relocate to the spleen (Figure 3). Additionally, the treated responder rats did not show any sign of illness even though the carrier was present in the spleen likely due to the *msbB* mutation that limits its ability to elicit systemic toxicity.[23]

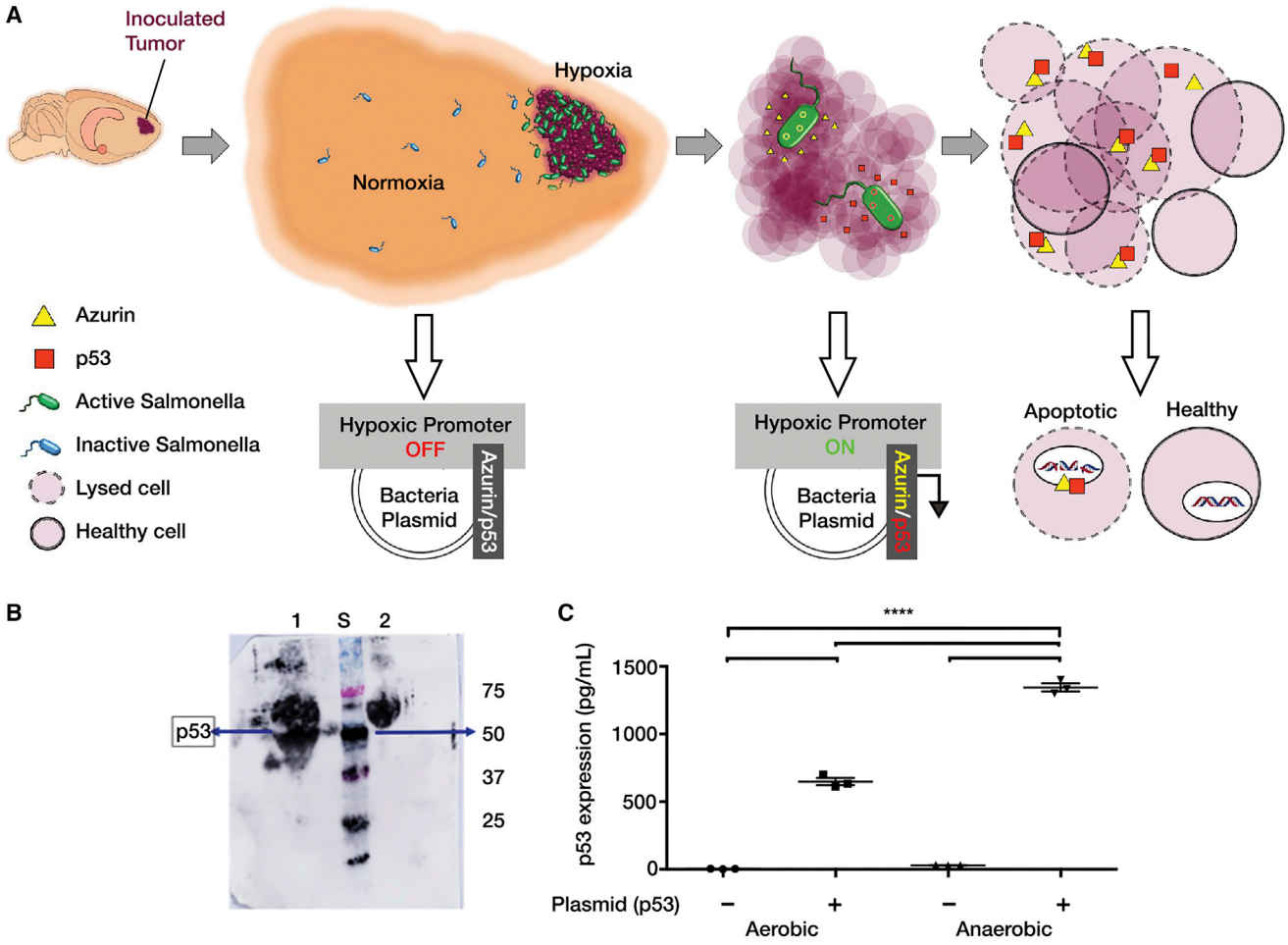

Figure 1. Bacterial Carrier Design

(A) Schematic showing hypoxia-inducible expression of p53 and Azurin within the tumor by carrier where conditions are hypoxic compared to the surrounding healthy tissues, thus causing selective apoptosis within tumor cells. (B) Western blotting showed relatively greater expression of p53 (around 50 kDa) in vitro when the carrier was grown anaerobically (lane 1) compared to when grown aerobically (lane 2). STDs (S) used: precision plus protein dual-color standards from Bio-Rad. (C) ELISA showing relatively greater expression of p53 when carrier was grown anaerobically compared to when grown aerobically in vitro. Control used is carrier without the expression plasmid. Mean ± SEM shown.

In the treated non-responder rat brain, a number of carriers were detected within the tumor region, with minimal detection in the surrounding healthy tissue. This indicates that bacterial carriers could easily migrate throughout the tumor and preferentially colonize it compared to the surrounding tissue. The spleen and liver of treated non-responder rats did not show presence of the carrier (Figure 3).

VNP 20009 Strains Were Recovered from Brains of Immunocompetent Rats

The colony counts obtained from rat brains (n = 3, without tumor inoculation) on day 15 after bacterial injection were at least 10-fold higher relative to the number of bacteria inoculated. This indicates that the strain survives even when challenged by host immune response.

Carrier Injection Did Not Elevate TNF-α Levels in Blood, Brain, Spleen, and Liver of Treated Rats, Indicating Absence of Systemic Toxicity; Apoptosis Was Not Observed in Liver and Spleen

Although strains of *S. typhimurium* have been used as anti-cancer agents for treating a variety of cancers,[54] one potential concern is their ability to induce systemic toxicity via the endotoxic lipid A membrane component. To mitigate this risk, VNP20009 strain was chosen because it is deficient in the lipid A component.[23] A 3,3′-diaminobenzidine (DAB) peroxidase staining was performed with anti-TNF-α antibodies on brain, liver, and spleen sections to check for levels of TNF-α as an indicator of systemic toxicity. No difference was observed between the three groups (Figure 4A). To further rule out any signs of systemic toxicity in carrier-injected rats, an ELISA was performed on the serum (collected post-euthanization) to check for

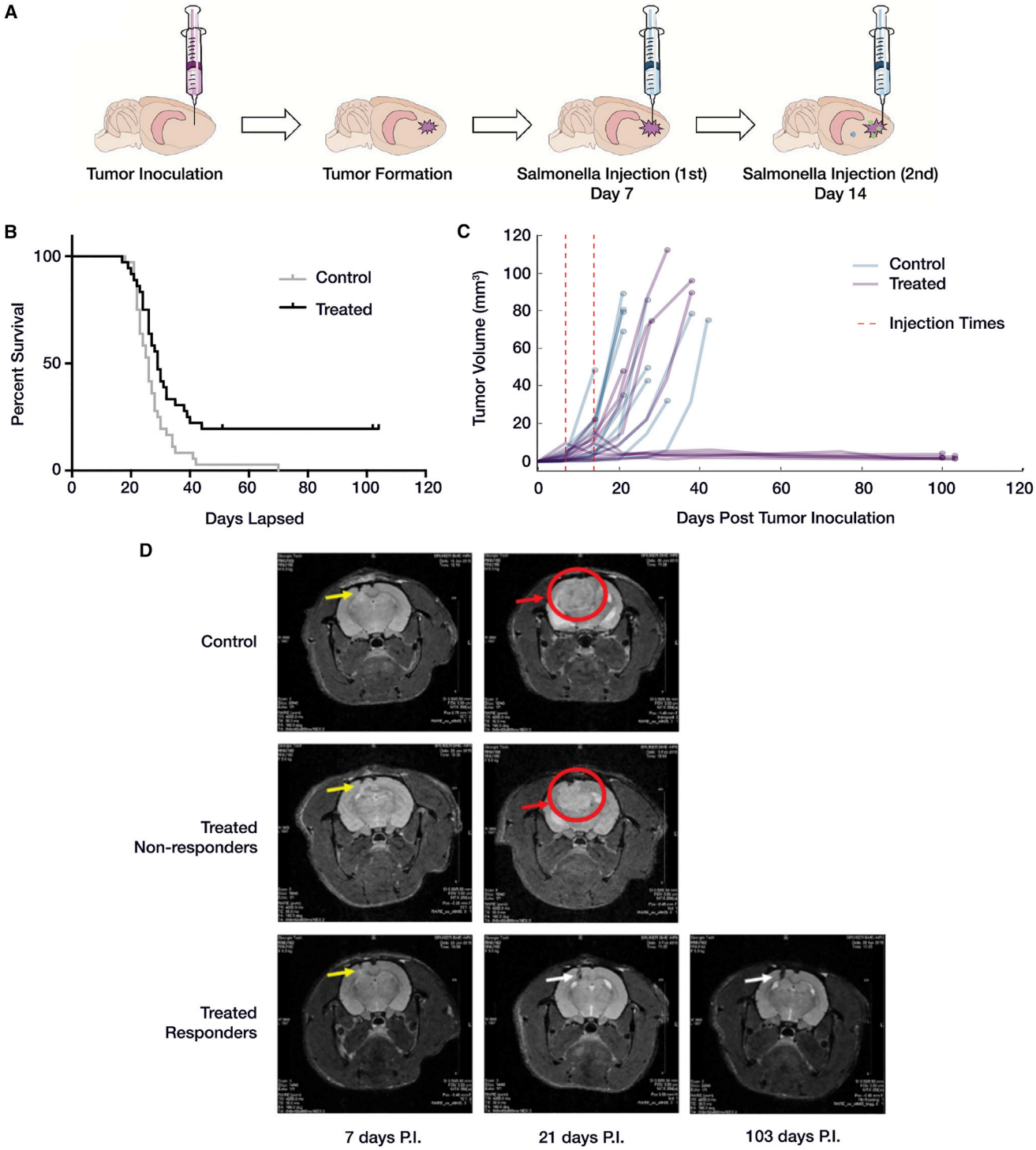

Figure 2. In Vivo Outcomes of Bacterial Carrier Therapy

(A) Schematic showing timeline of intracranial tumor implantation followed by injection of carrier at the same site of tumor implant after 1 week. Two injections of carrier were given a week apart from one another. (B) Compiled Kaplan-Meier plot for control (sham injected, n = 36) and treated rats (injected with carrier expressing Azurin plus p53, n = 36). Results showed around 19.4% survival in treated rat group (responders) with survival extending beyond 100 days. Log rank Mantel-Cox test p value = 0.0046. (C) Tumor volumes calculated from MRI images for two sets of experiments involving control (n = 12) and treated (n = 12) rats. Tumor volume increased exponentially in all the

(legend continued on next page)

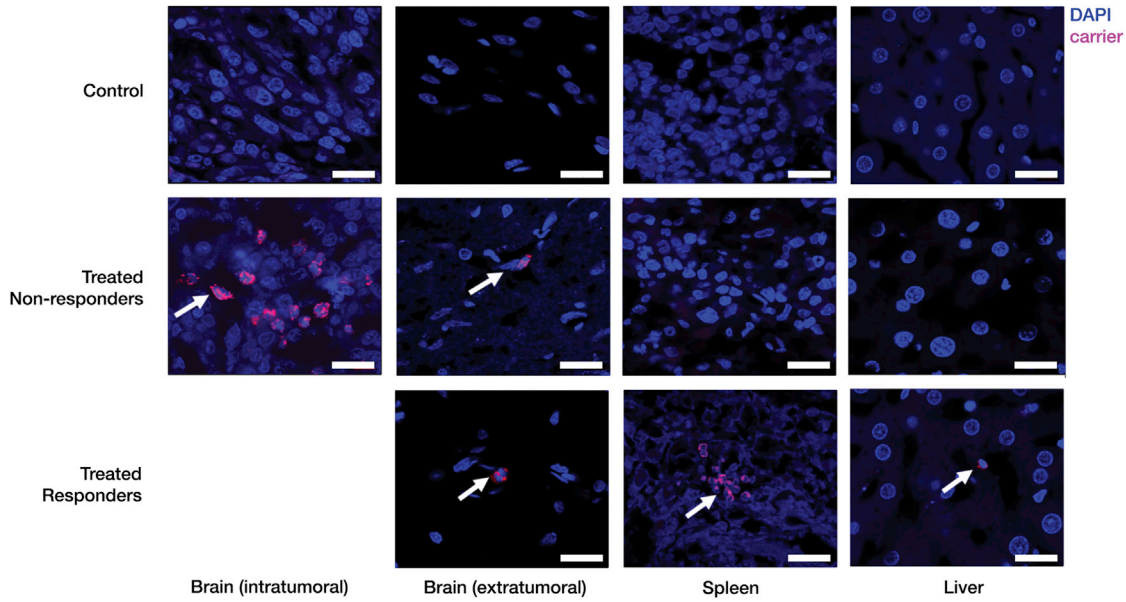

Figure 3. Biodistribution of Bacterial Carriers

Fluorescent in situ hybridization (FISH) to detect carrier (pink) in the brain, spleen, and liver of treated non-responder and treated responder rats (the latter, euthanized on day 104). A number of carrier cells were present *inside the tumor* of treated non-responder rats (white arrows), with negligible number in the surrounding healthy tissue. Carriers were not observed in the spleen and liver of treated non-responders. For responders, significantly few carriers were present in the brain and liver. Carriers were detected in the spleens of responders (white arrows). Scale bars, 20 μm.

levels of TNF-α. It was seen that TNF-α levels were comparable between control, treated responder and non-responder rats (Figure 4B). Terminal deoxynucleotidyl transferase dUTP nick end labeling (TUNEL) staining performed for liver and spleen of control, treated non-responder, and responder rats did not show any signs of apoptosis (Figure 4C).

p53 Is Present in Non-responder Tumors and Coincides with Expression of Pro-apoptotic markers, but Also Proliferative Ones

Fluorescent staining of brain sections using anti-p53 antibodies (Figure 5A) showed greater levels of p53 in treated non-responder rats compared to control rats, although the difference was not statistically significant (Figure 5B). Unfortunately, fluorescent staining for Azurin was not technically possible due to commercial unavailability of anti-Azurin antibodies.

To investigate whether expression of p53 and Azurin led to changes in the extent of apoptosis, immunohistochemistry (IHC) with anti-cleaved poly-ADP ribose polymerase (PARP) antibodies (indicator of apoptosis) and TUNEL assay were performed. Extent of PARP staining within tumors (Figure 5C) was slightly greater, but not significant in treated non-responder rats compared to the control rats ($p < 0.6944$) (Figure 5D). However, treated non-responder rats showed an 8- to 10-fold increase in the number of TUNEL-positive cells within the tumor region compared to the control rats ($p < 0.1149$) (Figures 5E and 5F). This indicates that the expression of p53 and Azurin increased the extent of apoptosis in treated non-responder rats. In Figure S2, DAB staining of tumor from a treated non-responder rat showed increase in p53 levels (expressed by carrier) and an influx of activated microglia (innate immune response) near the carrier injection site, which coincided with increased PARP (greater apoptosis) and decreased ki67 (less cell proliferation) staining. However, increased ki67 was observed in the region surrounding the carrier injection site.

One of the treated rats that after carrier inoculation did not show tumor growth per MRI was euthanized early on day 52. The brain sections of this rat showed slightly greater number of tumor cells compared to the ones euthanized on day 104 (Figures S3A–S3C), but the number was severalfold lower compared to control and non-responder rat brain (Figures S3D and S3E). The treated responder brain sections at day 52 showed positive staining for p53, PARP, and TUNEL within the tumor region, indicating apoptotic responses exerted by the carrier (Figures S3A–S3C). This means that, in the treated responders, the tumor

control rats. In 6 out of 12 treated rats (responders), the tumor growth was suppressed, which led to increased survival. (D) Representative MRI images of brain from control, treated non-responder, and responder rats. Yellow arrows show tumor implant site, which is the same site for carrier injection. In the control and treated non-responder rats, tumor continued to grow as shown here on day 21 post-tumor implant (PI) (red arrow). However, in some of the treated rats, the tumor growth was suppressed (responder), and only slight inflammation was observed at needle site on day 103 PI (white arrow).

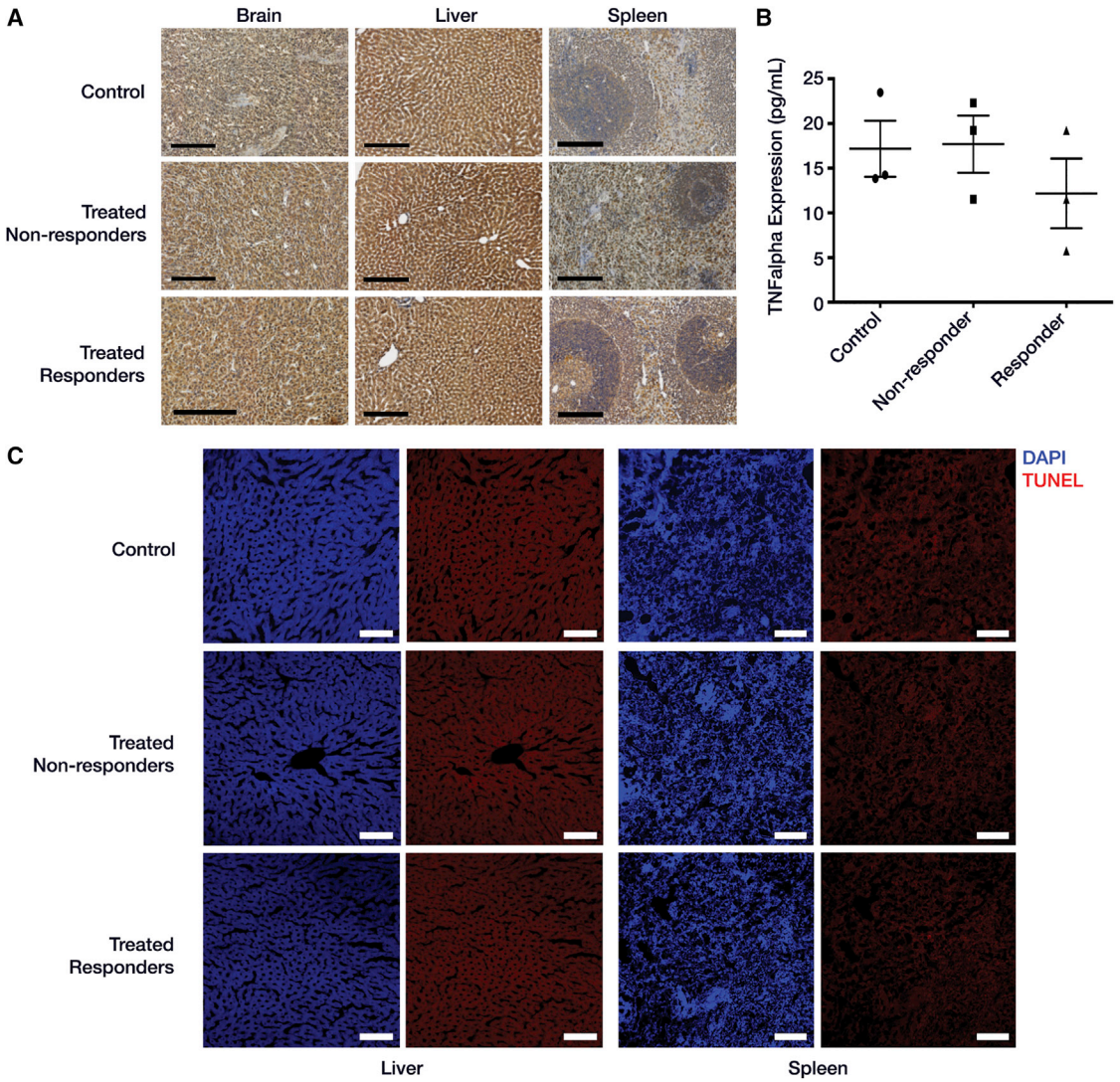

Figure 4. Bacterial Carriers Exhibit Lack of Systemic Toxicity

(A) DAB staining with anti-TNF-α (indicator of systemic toxicity) for brain, liver, and spleen sections from control, treated non-responder, and responder rats looked comparable. (B) TNF-α levels were comparable and not significantly different in serum from control, treated non-responder, and responder rats as observed in ELISA (n = 3 for each group), indicating no increase in systemic toxicity due to carrier treatment (ANOVA, alpha = 0.05, Tukey multiple comparisons; control versus non-responders: p = 0.9939; control versus responders: p = 0.5867; non-responders versus responders: p = 0.5291). Mean ± SEM and pre-averaged biological replicates shown. (C) TUNEL staining showed absence of apoptosis within spleen and liver of control, treated non-responder, and responder rats. DAPI (blue), TUNEL (red; however, what is shown above contains only background). Scale bars, 200 μm (black) and 100 μm (white).

population continues to diminish in response to the treatment, and later reaches undetectable levels as time elapses (Figure 6A). PARP and TUNEL expression were not observed in p53-negative tissues including adjacent extratumoral brain tissues.

Proteomic and Pathway Analyses Show Similar Protein Expression between Both Controls and Non-responders, but Dramatically Different Expression Profile for Responders

A cohort of 12 animals with 6 controls, 3 treated non-responders, and 3 treated responders was used for proteomic analysis to further understand the mechanism of action of these tumoricidal carriers (Figures S4A and S4B). An average of 60,006 peptide spectrum matches (PSMs) per sample were assigned to 4,980 uniquely identified proteins (associated with a unique UNIPROT accession ID) and used for further analyses. Hierarchical clustering using Euclidean distance of the set of PSMs (Figure S4D), showed that the responder group relative to both control and non-responder groups were distinctly clustered, whereas the non-responder and control group were more closely related as two of the controls clustered better with the non-responders than with the other controls.

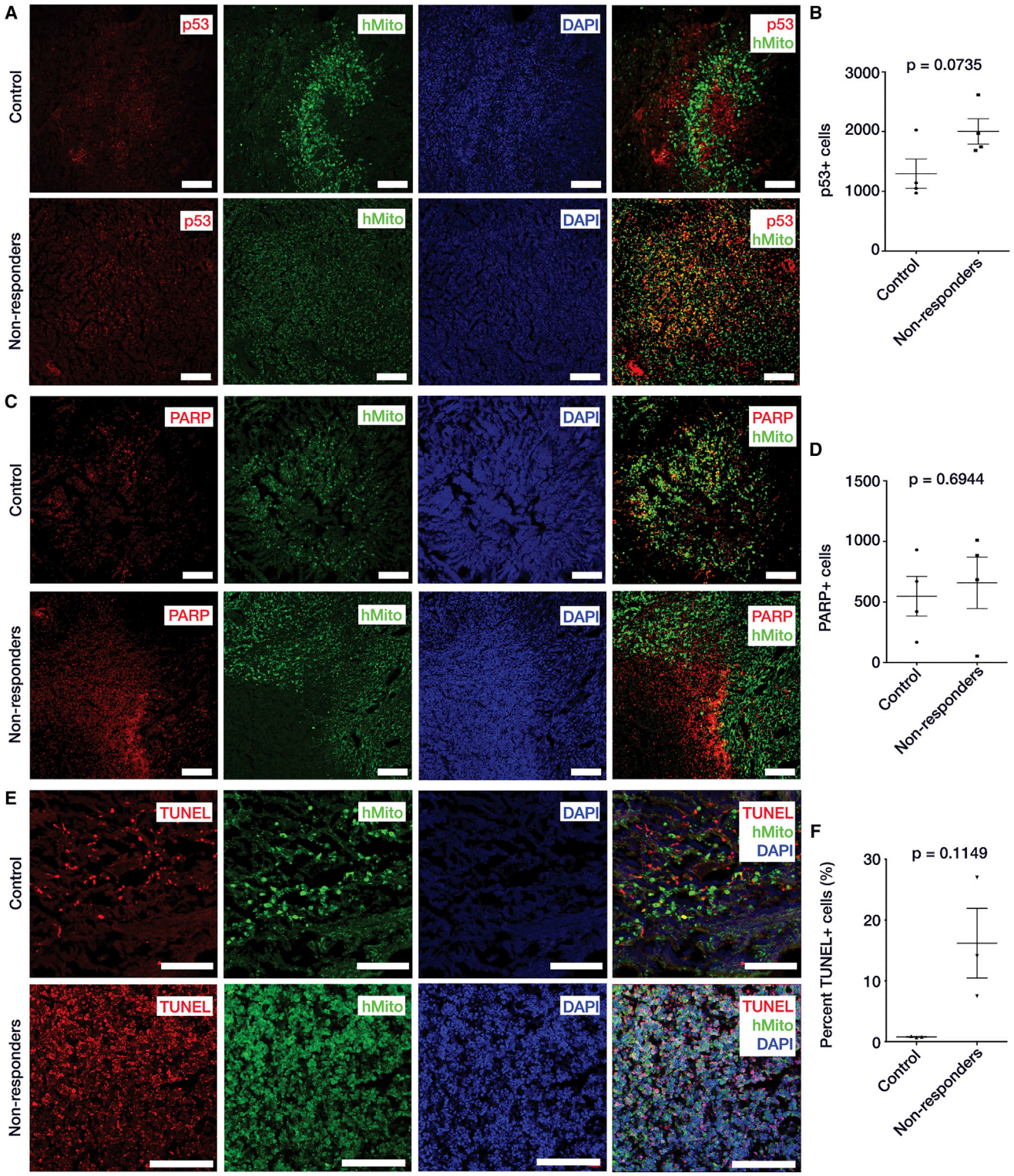

Figure 5. Immunohistochemistry of p53-Mediated Apoptosis after Bacterial Carrier Therapy

(A) IHC images of brain sections from control and treated non-responder rats to check for expression of p53. Green, human anti-mitochondria antibodies that specifically stain tumor cells derived from U87MG human tumor cell line. Blue, DAPI; and red, p53. More p53 observed within tumor of treated non-responder rats compared to control.

(legend continued on next page)

Statistical analysis was performed and used to define differentially expressed (DE) proteins by filtering for ±2-fold change between conditions and applying a false-discovery rate (FDR) threshold at 0.05. In total, 2,459 differentially expressed proteins were found between the responder and control groups, 2,027 from the responders and non-responders, but only 186 proteins were differentially regulated between the non-responder and control groups (Figure S4C). Table S3 shows the top 20 up- and down- regulated of these proteins between each condition pair. (For complete dataset, please see Data S1, S2, and S3.) The Euler diagram in Figure S4E depicts how these DE proteins group among conditions and whether they were relatively up- or down-regulated for each condition pair clearly showing a large overlap in proteins that are differentially expressed in responders relative to both control and non-responders. The smallest subsets were for non-responders relative to controls, with only eight up-folded DE proteins in total.

To determine which protein signaling pathways were differentially expressed between treatment conditions, pathway overrepresentation was measured using each of the differentially expressed protein sets. Due to the fact that this study uses a xenograft model and the protein accessions were assigned parsimoniously without guarantee of correct species being attributed, this analysis opted to use the related gene symbols instead of protein accessions and performed the lookups against human databases only. Human databases are more thoroughly annotated than those for rat model used in this study, and therefore more accurate for assessing response of human GBM model. The search elicited 284 significantly (by g: SCS threshold) overrepresented pathways for the non-responder:control condition pair, 2,172 for responder:control, and 2,347 for responder:non-responder.

Further inquiry into differential pathway expression was determined using gene set enrichment analysis against the Gene Ontology and Reactome datasets. This was performed using the log2 fold change for all measured proteins between each condition pair as the pre-ranked metric. The five highest and lowest normalized enrichment scores for each condition pair are shown in Table S4. Between the non-responder:control condition pair, only 13 gene sets were found to be significantly enriched in non-responders with an FDR of < 25%, and 8 were significantly enriched in controls. For the responder:control pair, 185 gene sets were significantly enriched in responders and 255 in control. Finally, for responder:non-responder, 146 enriched in responders and 132 in non-responders. These significantly enrichment networks for responder:control and non-responder:control shown in Figure S5. Due to the large distinction between responders and controls, the enrichment map for responders (Figure S5A) is vast. Apparent are groupings of positive enrichment associated with mitochondrial function and biogenesis, transmembrane transport, and neuronal signaling, as well as nervous system development. The connectivity of negatively enriched pathways for responders is less clear, likely due to the overall decrease in tumor cells present in these samples. If there were a significant number of tumor cells present, a diverse positive enrichment in pathways for metabolic processes would be evident. Instead, in the responder network, a negative enrichment for a number of pathways related to protein translation and cell cycle processes was seen. Of the few significantly enriched pathways in non-responders (Figure S5B), most were associated with either ribosomal function, or protein folding and assembly.

Treated Responders Lack Indication of Residual GBM Tissue and Are Enriched with Pro-neural Proteins

In the treated rats that were euthanized after more than 100 days, only a sparse population of dispersed tumor cells was observed in brain sections stained with an anti-mitochondria antibody specific for human cells (Figure 6A). This is a dramatic contrast to the other outcome cohorts, as the tumor population from both the control (Figure S3D) and treated non-responder (Figure S3E) rats was dense with positive human mitochondria staining.

Many neuro-related pathways were found in both the overrepresentation and enrichment analyses for responders. In particular, the ontology for Neuron Parts (GO: 0097458) showed considerable increase in expression in the responders for peptides that were parsimoniously assigned to rat proteins (Figure 6B). Figure 6C shows several other neuronal pathways, all significantly overrepresented by the DE proteins in responders relative to controls. All but the neuron projection extension pathway showed a clear bias for up-regulated proteins. The gliogenesis pathway was also significantly overrepresented; however, the split between DE up- and down-regulation was mixed, likely indicating both a loss of GBM-related proteins and renewal of a healthy glial cellular milieu. Wound healing (GO: 0042060) and apoptotic processes (GO: 006915) were both biased for down-regulation in the responders, further indicating a renewed neural environment.

(B) Quantification of IHC images showed greater p53 levels in treated non-responder rats compared to control rats with p value of 0.0735. Nine images were taken from each control (n = 4) and treated non-responder rat (n = 4) for this analysis. (C) IHC images of brain sections from control and treated non-responder rats to check for presence of cleaved PARP (indicator of apoptosis). Green, human anti-mitochondria antibodies; blue, DAPI; and red, cleaved PARP. There were more PARP-positive cells in treated non-responder rats compared to control. (D) Quantification of IHC images showed more cleaved PARP in treated non-responder rats compared to controls with p value of 0.6944. Nine images were taken from each control (n = 4) and treated non-responder rat (n = 4) for this analysis. (E) TUNEL staining to check for apoptosis within tumor of control and treated non-responder rats. Green, anti-mitochondria antibodies; blue, DAPI; and red, TUNEL-positive cells. There were more TUNEL-positive cells in the tumor region of treated non-responders compared to control. (F) Quantification and statistical analysis of TUNEL taken from 18 different regions within each tumor of control (n = 3) and treated non-responder (n = 3) rats. TUNEL reaction in treated non-responders was 8- to 10-fold greater compared to control rats. All statistics were down by t test with Welch's correction, alpha = 0.05. Mean ± SEM and pre-averaged biological replicates shown. Scale bars, 100 μm.

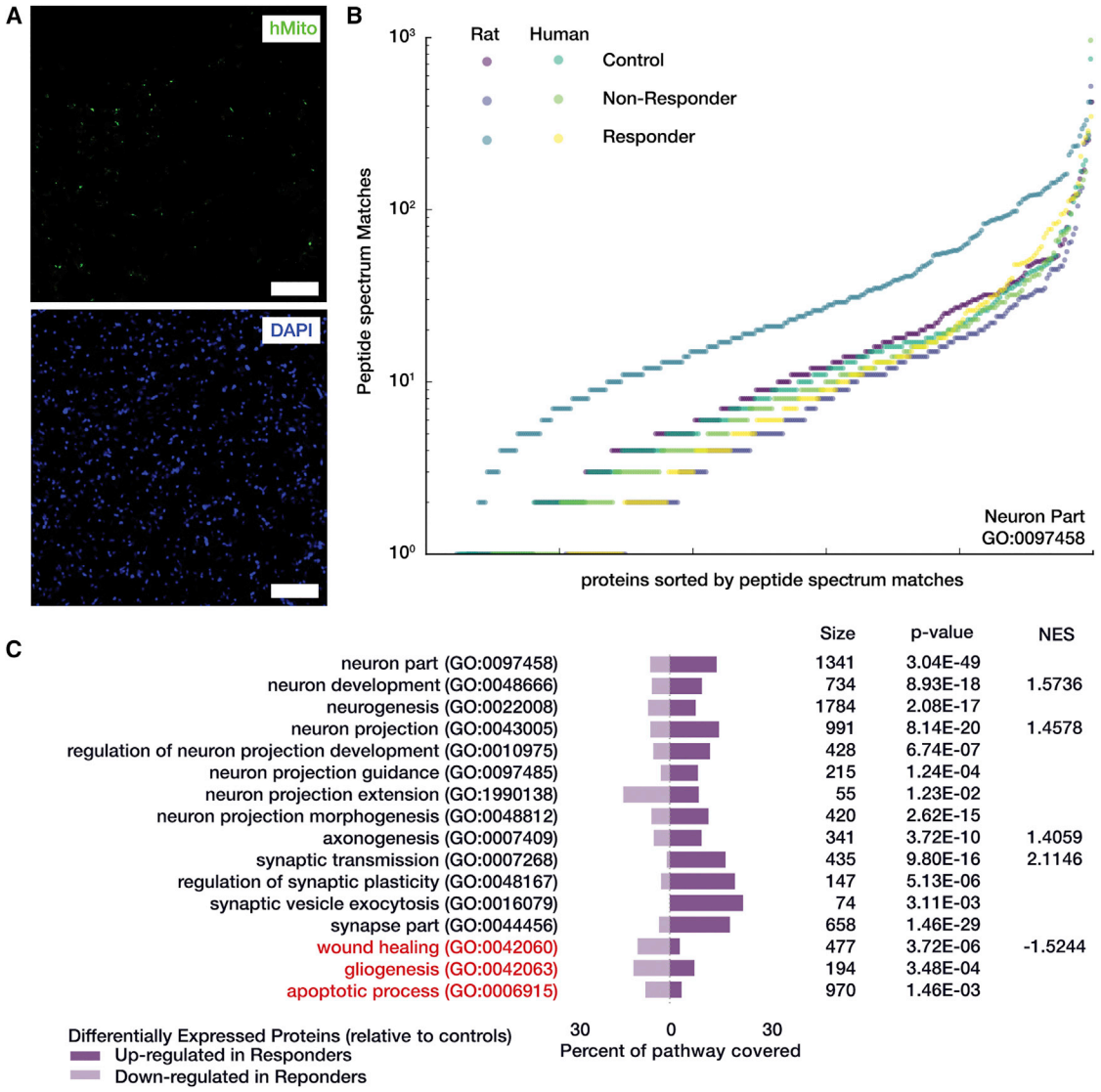

Figure 6. Proteomic Assessment of Bacterial Carrier Responding Cohort

(A) Human mitochondria antibody (green, top) and DAPI (blue, bottom) for treated responders showed a complete loss of GBM cells (cf. Figure 5). Images were contrast-enhanced digitally to improve visibility of low fluorescent signals. Scale bar, 100 μm. (B) Individual peptide spectrum match counts for proteins in the Neuron Part (GO: 0097458) ontology that were also measured by proteomics. Protein measurements are split by both outcome condition and species of protein assignment and sorted for cumulative display. Proteins that were measured as rat in the responder cohort were substantially more up-regulated overall than all other conditions. (C) Curated list of pathways over-representation analysis that emphasize a pro-neural protein signature. Bar graphs indicate the number of differentially expressed proteins that were measured via proteomics and also overlap with the related ontology and whether they were up- or down-fold relative to the control cohort. NES is the normalized enrichment score from gene set enrichment analysis used in this study, where a positive score indicates significant enrichment of the pathway in the responder cohort, whereas a negative score indicates a significant down-regulation of the pathway.

Protein Analysis Showed Differential Regulation of Both Pro- and Anti-apoptotic Proteins between Control and Non-responder Rats

In order to check for differences in the type and relative levels of apoptotic proteins in the tumors of non-responders and controls, a G-series apoptotic antibody array analysis was performed on the tumor lysate (RayBiotech AAH-APO-G1). Statistical analysis was not performed, as the biological replicates were pre-pooled before analysis; instead, relative fold change in expression is reported (Figure 7A). Twelve of these proteins were more than 2-fold up-regulated, whereas 5 were more than 2-fold down-regulated in non-responders relative to controls.

A BIOGRID[55] protein-protein interaction neighborhood was generated for the antibody array proteins and rearranged to emphasize connectivity with respect to p53. This network was colored from

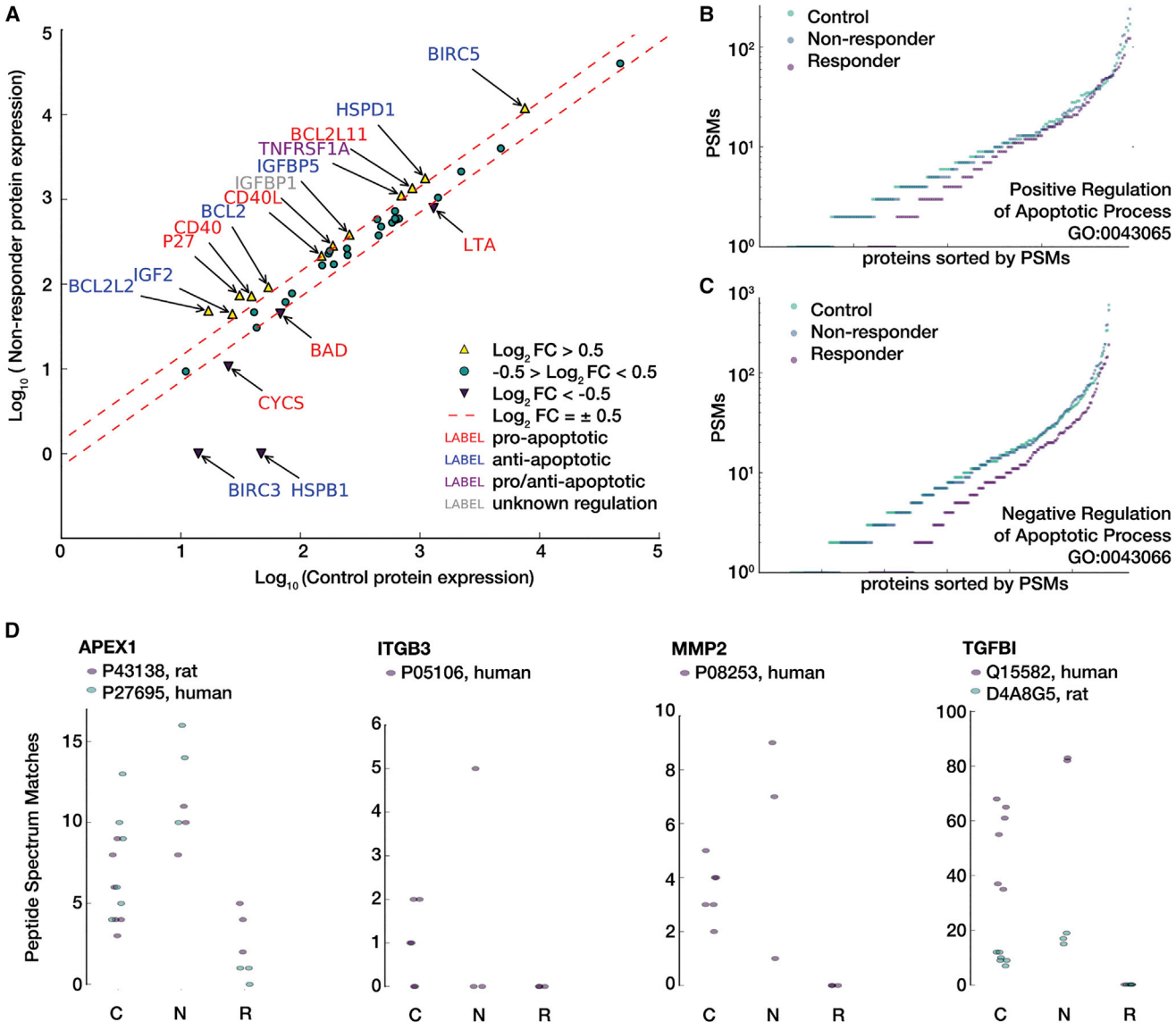

Figure 7. Proteomic Assessment of Bacterial Carrier Non-response

(A) Results from G-series apoptosis array to check for levels of apoptotic proteins in the tumor lysate from control and treated non-responder rats. Proteins with a ±2-fold change are annotated and colored depending on their regulation of apoptosis. Again, there appears to be no dramatic difference between the conditions, and for the majority of those proteins that are distinct, no clear positive or negative apoptotic regulation is clear. Shown next are individual peptide spectrum match counts for proteins in the ontologies for (B) positive (GO: 0043065) and (C) negative (GO: 0043066) regulation of apoptosis that were also measured by proteomics. Protein measurements are split by both outcome condition and sorted for cumulative display. Proteins that were measured in the responder cohort showed substantially lower expression than in controls and non-responder, both of which were relatively indistinguishable when looking at these overall pathway responses. (D) Peptide spectrum matches for posited therapy resistance protein markers. Up-regulation of APEX1, MMP2, and TGFBI, and down-regulation of ITGB3 are consistent with a drug-resistant phenotype in glioma. C, control; N, non-responders; R, responders.

relative protein expression and showed that p53-associated signaling in non-responders relative to controls (Figure S6A, proteomic and array data averaged) is dramatically different and not consistently up- or down-regulated. However, a comparison of responders relative to controls (Figure S6B, proteomic data only) exhibited a general down-regulation of all p53-associated proteins.

Figure S7 shows coverage of measurements used in this study on the Kyoto Encyclopedia of Genes and Genomes (KEGG)[56] canonical p53 Signaling (HAS: 04115) (Figure S7A) and apoptosis (HSA: 04210) (Figure S7B) pathways, colored using average non-responder fold change relative to controls, using proteomics and western array data. Moreover, when comparing the full set of proteins that either

positively or negatively regulate apoptosis (Figures 7B and 7C), non-responders and controls do not appear to be distinct; the related expression in responders, however, is generally lower when looking at these broad regulatory ontology sets.

DISCUSSION

Facultative anaerobic bacteria such as *S. typhimurium* have been previously shown to preferentially multiply in hypoxic and necrotic regions within a tumor.[24] This active tumor-targeting potential of bacteria has been previously exploited to express tumoricidal proteins that can induce apoptosis and suppress tumor growth in different cancer types.[57] The particular novelty of this study is the use of *S. typhimurium* to deliver a tumoricidal combination therapy of p53 and Azurin that synergistically induce apoptosis in an intracranial rat model of aggressive GBM tumor in the absence of an adjuvant therapy. In GBM, drug diffusion is a major impediment to successful treatment, and the motile phenotype of the bacteria is advantageous in that active delivery through the tumor can be achieved without any external pressure or chemical gradient, thus overcoming the difficulties encountered with CED. Additionally, use of bacteria as a carrier for plasmid-mediated expression of proteins affords improved programmability and sustained drug delivery compared to conventional gene therapies.

S. typhimurium is a known intracellular pathogen, and in particular, the VNP strain has been shown to express proteins in host tissues[53,58,59] (also observed in Figure 3). Once a VNP carrier invades the host cell, it can express Azurin, which gets secreted outside the bacterial cell into the host cytosol (due to its N-terminal secretion signal sequence) where it can exert its apoptotic activity or protect endogenously synthesized or bacterially expressed p53. In case of p53, although it lacks a secretion signal, p53 secretion was observed in vitro (Figure 1C) by an unknown mechanism. Furthermore, we observed that the levels of p53 in the host tissue that has the carrier is greater than in control rats (Figures 5A and 5B), indicating successful p53 expression and release. Once released, we hypothesize that p53 can express its apoptotic action within the cytosol by up-regulating proteins such as Bax that creates pores in mitochondrial outer membrane and starting the caspase cascade. Because we have used carriers to express wild-type p53, and this protein has an intact proline-rich domain and nuclear localization signaling domain, we hypothesize that cytosolic p53 can make its way into the nucleus in order to initiate additional apoptotic pathways.

Coincident expression of p53 and Azurin was required for a survival benefit in U87mg-xenografted rats (Figures 2B, S1A, and S1B). The inability of p53 alone to induce apoptosis in U87mg cells is consistent with previous work[60–62] showing that, although U87mg cells natively express wild-type p53, they are apoptotic resistant to induction of exogenous wild-type p53 alone. Furthermore, p53 is a labile protein and by itself is subject to ubiquitination and proteasomal degradation, with a half-life of approximately 25–30 min if left unprotected.[46–48] Hence, Azurin was co-expressed with p53 in order provide the requisite stabilization.

To mitigate concerns over the use of tumoricidal carriers and their potential impact on healthy tissues and host response, we have opted for an avirulent carrier, *S. typhimurium*, VNP 20009, and in addition, engineered expression of apoptotic proteins to be regionally limited. Azurin- and p53-encoding genes were cloned downstream of a hypoxic promoter, *pflE*, which has been shown in previous studies to offer dual advantages: (1) it is a microaerobically induced, which means that is greatly induced under hypoxic conditions compared to normoxic conditions; and (2) this promoter has been shown to turn "on" genes only within tumors and not in other tissues,[52,53] thus avoiding unintended toxicity to healthy tissues.

The prolonged preferential presence of the bacteria within the tumor, and the hypoxia-dependent production of p53 and Azurin allow sustained expression of the proteins of interest in the region of interest. As observed in treated non-responders (Figure 3), the carrier localized mainly to the tumor with minimal presence in healthy tissues, indicating that the nutrient-rich, immunosuppressed microenvironment of the tumor provides a preferential location for the carrier to reside and multiply.[24] Even with a baseline p53 expression under normoxic conditions (Figure 1C), p53 expression and p53-mediated apoptosis were not observed in the adjacent healthy brain tissues (Figures S3A–S3C). Importantly, even with this sustained presence of a foreign organism, treatment with the carrier does not appear to directly compromise animal safety, as none of our surviving animals showed bacteria-associated symptoms of diminished health or systemic toxicity as indicated by TNF-α levels in the blood (Figure 4).

Previous studies have shown that these carriers are quickly cleared from the bloodstream either due to the phagocytic action of polymorphonuclear leucocytes, or via the reticuloendothelial system of the liver and the spleen, thus alleviating the overall infectious state of the animal.[63–65] In addition to the multiple host mechanisms enabling clearance of the bacteria, the carriers can also be cleared by administration of an antibiotic, such as tetracycline and enrofloxacin.[23]

Our compiled in vivo tumor implant studies demonstrate that, in 19% of treated rats, the tumor growth was retarded and the rats survived for more than 100 days (Figure 2B). In the treated rats, the response was discretely either therapeutic or not. Decrease in tumor volume was only seen in the survival cohort, and the indication of tumor regression was tied directly to the measurement following either the first or second injection of carrier. The fact that some animals did not show a therapeutic response until after the second injection is important to note, as it suggests that increasing the number or altering the schedule of injections may be sufficient to produce an improved response rate.

In the responding animals, we found only trace evidence of GBM cells histologically (Figure 6A). Proteomic analysis clearly showed a restored neural environment as evident by the numerous pro-neural pathways that were either overrepresented or enriched in responders relative to both treated non-responders and controls (Figures 6B and 6C). This is a strong indication that there is a significantly large

representation of neuronal cells in the responder tissue, likely due to a lack of GBM cells. The global protein signatures for responders are also very distinct from both the non-responders and controls (as seen in terms of PSM distance; Figure S4D). In contrast, when using this same distance metric and even when looking at the signaling pathways for positive and negative regulation of apoptosis (Figures 7B and 7C), non-responders and controls are essentially indistinct. This is confirmed by more sensitive antibody-based measurement of particular apoptosis-associated proteins seen in Figure 7A. Differentiating these proteins by pro- and anti-apoptotic function also elucidates no clear trend in overall apoptotic regulation. For instance, BIRC3 and HSPB1, both anti-apoptotic proteins are substantially down-regulated in non-responders, but so is CYCS, a key p53-mediated, pro-apoptotic initiator. However, this ambiguous response is not necessarily surprising, given that we observed increased TUNEL-positive expression (Figures 5E and 5F) in the non-responders (indicating pro-apoptotic processes) yet did not see tumor regression overall in those animals via both MRI-measured tumor volume (Figures 2C and 2D) and in terms of survival (Figure 2B).

When looking specifically at the p53-mediated protein network, however, there are considerable differences between the non-responders and controls. To explore the regulation of apoptosis as centered around p53, a BIOGRID[55] protein-protein interaction neighborhood was generated for these apoptosis-associated proteins that were colored using the combined array and proteomic data for non-responders relative to controls (Figure S6A). Within this network, there was a dramatically different p53-associated signaling in non-responders relative to controls, suggesting that there is a differential regulation of p53 in these animals. At least, this seems to indicate a perturbation in p53-associated signaling in response to the carrier even if it is not robust for pro-apoptosis. In contrast, the responders appear to be generally down-regulated across the p53 neighborhood relative to controls (shown using only proteomics data in Figure S6B) likely due to the lack of active carriers once the tumor is depleted.

Last, we investigated the protein data for indications of compensatory mechanisms, other than those that are directly anti-apoptotic, that exhibited a drug resistance-like response in non-responders. Although many key glioma drug resistance markers were not detected (e.g., MDR1, MRP, LCN2), Figure 7D shows the peptide spectrum matches for four proteins that were detected via proteomics of particular note. APEX1, an endonuclease associated with gliomagenesis that is known to be correlated with reduced therapeutic efficacy in glioma,[66] showed an overall increased expression in non-responders. MMP2, a collagenase that can be transcriptionally activated by p53[67] and is associated with enhanced tumor growth in glioma[68] showed a dramatic increase in two of three non-responders. Both accession identities for TGFBI, another indicator of glioma invasiveness[69] that may be secreted in drug-resistant glioma,[70] showed relative increase in expression. Last, ITGB3, an integrin component that is known to be down-regulated in drug-resistant gliomas,[69] was undetected in two of three non-responders.

Even with this detailed proteomic analysis, no solely pro- or anti-apoptotic signal in the non-responders could be resolved. The lack of spatial discrimination and temporal resolution of the protein analyses may have contributed to the ambiguous evidence of apoptotic regulation. Temporal resolution was limited mainly due to lack of non-invasive measurement of tumor progression other than MRI and no direct measurement of apoptotic signaling in situ until after the animal is euthanized. Furthermore, without clear predictive outcomes, we could not reliably sacrifice an animal early knowing that the animal would be in the survival cohort or not. We were, however, able to sacrifice one suspected responder early at day 52, but this was done in a late cohort after we had established that animals surviving past day 40 were likely responders. With respect to spatial factors, treated non-responder status could be due to the phenotypic heterogeneity of the cell population as the tumor grows in its immunosuppressed environment and adopts a number of intrinsic and acquired mutations, with which tumors easily develop resistance to a number of therapeutic agents.[71] This may explain why, although in some parts of the treated non-responder rats the tumor underwent apoptosis, in other parts the tumor grew rampantly, resulting in increased tumor growth. The increased rate of tumor cell proliferation may have also impacted the extent of apoptosis as evident in Figure S2. Although ki67 staining is decreased directly near the carrier injection site, in the surrounding region, the tumor cells continued to grow. This indicates that, even though a therapeutic response is seen, it may be constrained regionally and can be overcome by the rate of tumor proliferation.

In conclusion, 19% of treated rats showed clearance of aggressive GBM. The treated non-responders demonstrated tumoricidal action via the engineered bacterial carriers as evident from multiple lines of analyses including immunohistochemistry and proteomics. The proteomic signatures suggest a complex response to the carrier therapy in non-responder animals and incontrovertible evidence for tumor clearance in the treated responders. Importantly, the carriers were safe, with no evidence of any systemic toxicity. The evidence of apoptotic action of p53 and Azurin suggest that motile carriers represent versatile approach to expressing multiple tumoridical proteins in brain tumors.

MATERIALS AND METHODS

Construction of Azurin- and p53a-Expressing Carrier under the Control of Hypoxic Promoter

The *pflE* promoter that is upstream of the gene encoding pyruvate formate lyase in *S. typhimurium* was amplified from genomic DNA of this bacterium using primers PflE-F and PflE-R, and cloned in place of the lacZ promoter in pDSRed2 plasmid (Clontech). This was followed by deleting DSRed2 gene and replacing it with either gene encoding p53 (using primers p53-F and p53-R) or Azurin (using primers Azurin-F and Azurin-R). Source of p53 was pUNO1hp53a plasmid (InvivoGen), and that of Azurin was genomic DNA of *Pseudomonas aeruginosa* PAO1. The pPflE-p53 and pPflE-Azurin cloned plasmids were individually transformed into chemically competent *S. typhimurium* strain VNP 20009 (ATCC 202165). Positive

transformants were confirmed by PCR. Primer sequences are given in Table S1. Expression of p53 and Azurin from aerobically and anaerobically grown bacteria (carrier) harboring pPflE-p53 or pPflE-Azurin plasmid was confirmed by western blotting or Mass Spec, respectively. Expression of p53 was also confirmed by ELISA.

Tumor Implant Protocol in Athymic Nude Rats followed by Intracranial Injection of Carrier Expressing p53 and Azurin

All animal procedures were conducted in accordance with Georgia Tech's Institutional Animal Care and Use Committee (IACUC). Adult male athymic RNU rats from Charles River laboratories were anaesthetized with inhaled isoflurane (2%–2.5%) and fit onto a stereotaxic device. A burr hole was drilled 2.0 mm lateral and 2.0 mm anterior to bregma to a depth of 2.0 mm in the left cortex. A 26G Hamilton needle was used to inject 80,000 human U87 MG GBM cells (ATCC HTB-14) into the drilled hole in a total volume of 5 μL at a rate of 1 μL/min. The drilled hole was closed using bone wax and the skin flap of the brain sutured. Upon detection of a small tumor in MRI after a week, one set of rats was injected at the site of tumor implant (ic) with 5 μL of carrier strains expressing p53 and Azurin grown individually and mixed 1:1 just before the injection (approximate count of each strain, 5×10^6 cells). This set of treated rats were injected (ic) one more time a week later with the same two strains. The control rats were injected with 5 μL of saline (ic). MRI was done weekly until the time of euthanization.

MRI Imaging to Check for Tumor Formation

The athymic nude rats were anaesthetized and placed in a Bruker Pharmascan 7-T (Bruker BioSpin MRI) operating with the ParaVision software with a 38-mm quadrature-detection volume coil as head coil. The animal was anaesthetized using 2% isoflurane and placed in a home-built cradle, allowing the easy placement of the animal's head within the MRI coil. The rapid acquisition of high quality T2 weighted images was achieved using the rapid imaging with refocused echoes (RARE) sequence (RARE factor, 6; effective echo time, 36 ms; repetition time [TR], 4,200 s; two averages per scan; total acquisition time, 6 min). A slab of 40 transversal slices was recorded using a field of view of 40 mm × 40 mm with a 256 × 256 matrix and a slice thickness of 0.5 mm. This slab was aligned to cover the injection site of the tumor cells using a pilot scan, which was recorded immediately before the acquisition of the RARE images. MRI was done every week following tumor implant to check for tumor growth or regression.

Tissue and Blood Collection for Protein Work, ELISA, and IHC

All euthanization and tissue-harvesting procedures were conducted in accordance with Georgia Tech's Institutional Animal Care and Use Committee (IACUC). Animals that showed clinical signs of illness were anaesthetized using ketamine (50 mg/kg), xylazine (10 mg/kg), acepromazine (1.67 mg/kg) cocktail. Then they were transcardially perfused with either sterile PBS (for protein work and ELISA) or with 4% paraformaldehyde (for IHC). The brain was harvested and transferred into liquid nitrogen or 10% buffered formalin, depending on tests to be performed. Some part of the tumor tissue (from control and treated non-responders) and part of the brain tissue (from treated responders) were sent for proteomics to Emory Core Proteomics Lab. The liver and spleen were harvested and stored in 10% buffered formalin. Blood from the heart was collected as a terminal procedure by using cardiac puncture technique. Serum was separated from the blood and used for ELISA.

Fluorescent in Situ Hybridization to Check for Presence of Carrier

To check for presence of carrier in brain, liver, and spleen, the tissue was sectioned to 7-μm thickness. The sections were permeabilized and hybridized with fluorescently labeled probe (Table S1) that binds specifically to the 23S rDNA of *S. typhimurium* at 46°C for 2 hr using a protocol as previously described.[72] Sections were then counterstained with DAPI. Images were viewed using the Zeiss LSM 700-405 confocal microscope.

Recovery of VNP 20009 from Immunocompetent Sprague-Dawley Rat Brains

Rats (n = 3) were injected intracranially (left cortex) and intravenously (tail) with VNP 20009. These rats did not have tumor inoculation. After 15 days, rats were euthanized and brains were homogenized and streaked on bacterial plates. Following 24-hr incubation, the colonies were counted.

ELISA to Check for Levels of TNF-α in Serum as an Indicator of Systemic Toxicity

Blood collected from heart was centrifuged at 1,000 × *g* for 10 min to separate the serum. TNF-α level in the serum was measured using anti-TNF-α ELISA kit as per the manufacturer's instructions (BD Biosciences).

Immunohistochemistry to Check for p53, Cleaved PARP, TNF-α, ki67, and CD68

To check for levels of p53 expression and cleaved PARP (indicator of apoptosis), the tissues were sectioned to 14-μm thickness, fixed with 4% paraformaldehyde, and blocked with blocking buffer for 1 hr. This was followed by treating with anti-p53 (Sigma; P 8999) or anti-cleaved PARP (Thermo Fisher Scientific; 44-698G) antibodies overnight in blocking buffer. On subsequent day, the sections were treated with fluorescent secondary antibodies. Sections were imaged on a Zeiss LSM 700-405 confocal microscope.

To check for levels of TNF-α (pro-inflammatory cytokine), ki67 (cell proliferation), CD68 (activated microglia), and cleaved PARP (apoptosis), the tissues were sectioned in 4- to 5-mm blocks and submitted as individual cassettes for paraffin embedding at Emory Winship Pathology Core Lab. Tissues from paraffin-embedded blocks were sectioned at 5-μm thickness. IHC was performed using DAB chromogenic kit (Wako) following the manufacturer's protocol. Antibodies used were anti-TNF-α (Boster Biologics; PA 1079), anti-p53 (Sigma; P8999), anti-cleaved PARP (Thermo Fisher Scientific; 44-698G), anti-ki67 (Thermo Fisher Scientific; MA5-15690), and anti-CD68 (AbD Serotec; MCA 341R). Whole-slide scanning was done using Hamamatsu's Nanozoomer 2.0 HT.

TUNEL for Brain, Liver, and Spleen Sections to Check for the Extent of Apoptosis

In Situ Cell Death Detection kit was used to label nicked 3′ ends with TMR-conjugated dUTP in order to detect apoptosis in tissue sections as per the manufacturer's instructions (Sigma).

Tissue Homogenization prior to Liquid Chromatography-Tandem Mass Spectrometry at Emory Proteomics Core Lab

Brain tissue was individually homogenized in 300 µL of urea lysis buffer (8 M urea, 100 mM $NaHPO_4$, pH 8.5) which had 3 µL (100× stock) of HALT protease and phosphatase inhibitor cocktail (Pierce). Homogenization was performed using a Bullet Blender (Next Advance) according to manufacturer protocols. Briefly, each tissue piece was added to urea lysis buffer in a 1.5-mL Rino tube (Next Advance) harboring 750-mg stainless-steel beads (0.9–2 mm in diameter) and blended twice for 5-min intervals at 4°C. Protein supernatants were transferred to 1.5-mL Eppendorf tubes and sonicated (Sonic Dismembrator; Fisher Scientific) three times for 5 s with 15-s intervals of rest at 30% amplitude to disrupt nucleic acids and subsequently vortexed. Protein concentration was determined by the BCA method, and samples were frozen in aliquots at −80°C. Protein homogenates (100 µg) were diluted with 50 mM NH_4HCO_3 to a final concentration of less than 2 M urea and then treated with 1 mM dithiothreitol (DTT) at 25°C for 30 min, followed by 5 mM iodoacetamide (IAA) at 25°C for 30 min in the dark. Protein was digested with 1:100 (w/w) lysyl endopeptidase (Wako) at 25°C for 2 hr and further digested overnight with 1:50 (w/w) trypsin (Promega) at 25°C. Resulting peptides were desalted with a Sep-Pak C18 column (Waters) and dried under vacuum.

Statistical Analysis

IHC comparisons were done in Prism 6 (for OSX; GraphPad Software) on pre-averaged biological replicates using a t test with Welch's correction for two group comparisons or ANOVA with Tukey multiple comparisons for comparisons across three groups (alpha = 0.05). Survival analysis was also done in Prism, using log rank (Mantel-Cox) to compare median survival across groups.

Liquid Chromatography-Tandem Mass Spectrometry Analysis at Emory Proteomics Core Lab

Brain-derived peptides were resuspended in peptide 100 µL of loading buffer (0.1% formic acid, 0.03% trifluoroacetic acid, 1% acetonitrile). Peptide mixtures (2 µL) were separated on a self-packed C18 (1.9 µm; Dr. Maisch) fused silica column (25 cm × 75 µm internal diameter [ID]; New Objective) by a Dionex Ultimate 3000 RSLCNano and monitored on a Fusion mass spectrometer (Thermo Fisher Scientific). Elution was performed over a 120-min gradient at a rate of 300 nL/min with buffer B ranging from 3% to 80% (buffer A: 0.1% formic acid in water; buffer B: 0.1% formic in acetonitrile). The mass spectrometer cycle was programmed to collect at the top speed for 3-s cycles. The mass spectrometry (MS) scans (400–1600 *m/z* range, 200,000 AGC, 50-ms maximum ion time) were collected at a resolution of 120,000 at *m/z* 200 in profile mode and the HCD MS/MS spectra (2 *m/z* isolation width, 30% collision energy, 10,000 AGC target, 35-ms maximum ion time) were detected in the ion trap. Dynamic exclusion was set to exclude previous sequenced precursor ions for 20 s within a 10-ppm window. Precursor ions with +1, and +8 or higher charge states were excluded from sequencing.

Spectra were searched using Proteome Discoverer 2.0 against human, rat, and *Salmonella* concatenated Uniprot database (134,326 target sequences). Searching parameters included fully tryptic restriction and a parent ion mass tolerance (±20 ppm). Methionine oxidation (+15.99492 Da), asparagine and glutamine deamidation (+0.98402 Da), and protein N-terminal acetylation (+42.03670) were variable modifications (up to three allowed per peptide); cysteine was assigned a fixed carbamidomethyl modification (+57.021465 Da). Percolator was used to filter the peptide spectrum matches to a false-discovery rate of 1%.

Proteomic Differential Expression

For proteomics, comparisons between fold changes of the PSMs were used to determine differential expression between the conditions. Data was pre-filtered (using Python; https://www.python.org/; https://www.scipy.org/) to eliminate samples where the PSMs were only non-zero for a single replicate across conditions. The statistical comparison tool QSPEC (v1.3.3)[73] (nburnin: 2,000; niters: 10,000; normalized: true) was used to compute a z statistic and FDR for each identified protein compared pairwise between conditions. The p values were obtained from the z statistic using R (http://www.R-project.org/). Proteins with a FDR < 0.05 for a particular fold change comparison between conditions were considered statistically significant and treated as DE for that condition-pair.

Pathway Overrepresentation Analysis

The DE proteins were pre-filtered (using custom Python code) to exclude proteins with a fold change less than 2-fold either up or down. For each condition-pair, gene ontology was performed using g:profiler version: r1536_e83_eg30 (http://biit.cs.ut.ee/gprofiler/).[74] Gene symbols were used indifferent to species attribution against the *Homo sapiens* dataset. The search included Gene Ontology, KEGG, Reactome, Regulatory Motif, Human Protein Atlas, CORUM, Human Phenotype Ontology, and OMIM databases and used the built-in g: SCS threshold for significance. Default settings were used. QuickGO (https://www.ebi.ac.uk/QuickGO) web service was used for obtaining additional gene ontology information for visualization with Python.

Pathway Enrichment Analysis

Gene Set Enrichment Analysis (GSEA) Build 0044 (http://www.broadinstitute.org/gsea)[75] was used to perform pathway enrichment analysis. Pre-ranked analysis was performed against the gene ontology (c5.all.v5.1.symbols.gmt) and Reactome (c2.cp.reactome.v5.1.symbols.gmt) datasets using the log2 fold change for all identified proteins as the ranking scheme for each condition-pair. Default setting were used except the max and min pathway size exclusion criteria were set to 1,000 and 5, respectively. Enrichment map

visualization was done using custom Python code and Enrichment Map, v2.1.0,[76] in Cytoscape, v3.3.0.[77]

RayBiotech G Series Western Array Blotting to Check Levels of Pro- and Anti-Apoptotic Proteins in Tumor Lysates

Tumor tissue from controls (n = 4) and treated non-responders (n = 4) were pooled in groups of two and homogenized in 1× cell lysis buffer (from Ray Biotech). Cell debris was removed by centrifugation at 1,000 × *g* for 10 min at 4°C. Total protein in the supernatant (lysate) was estimated using the BCA kit (Thermo Scientific). The 1,000 μg/mL lysate obtained from control and treated non-responder rat tumors was tested on G-series Human Apoptosis Array (AAH-APO-G1-4) using manufacturer's protocol, and analyzed using the RayBio analysis tool. g: Profiler was used to obtain a BIOGRID[55] neighborhood for the proteins measured on the array. Neighborhood network visualization was reconstructed using Cytoscape, v3.3.0,[77] and KEGG.[56]

SUPPLEMENTAL INFORMATION

Supplemental Information includes seven figures, four tables, and three data files and can be found with this article online at http://dx.doi.org/10.1016/j.omto.2016.12.003.

AUTHOR CONTRIBUTIONS

N. Mehta and J.G.L. prepared the manuscript and contributed equally to this work. N. Mehta designed and conducted the experiments. J.G.L. contributed proteomic, pathway, and general data and statistical analyses as well as conceptual and experimental design advice. K.P. contributed design and completion of staining and fluorescent in situ hybridization (FISH) assays, as well as broad technical assistance. N. Mokarram contributed conceptual advice, figure illustrations and manuscript revisions. C.K. contributed data quantification and interpretation for tissue histology and ELISA experiments as well as miscellaneous technical assistance. R.V.B. conceived the overall concept, contributed to experimental design, and supervised the project.

CONFLICTS OF INTEREST

The authors declare no conflicts of interest.

ACKNOWLEDGMENTS

This study was funded by generous support from Ian's Friends Foundation, Ann Rankin Cowan, Children's Healthcare of Atlanta, and Georgia Research Alliance. Furthermore, we would like to thank Dr. Tarun Saxena for his helpful discussion and valuable comments. Finally, we would like to thank Eric Gaupp, Radhika Patkar, and Anandita Ananthakumar for their excellent technical assistance.

REFERENCES

1. Johnson, D.R., and O'Neill, B.P. (2012). Glioblastoma survival in the United States before and during the temozolomide era. J. Neurooncol. *107*, 359–364.

2. Agarwal, S., Manchanda, P., Vogelbaum, M.A., Ohlfest, J.R., and Elmquist, W.F. (2013). Function of the blood-brain barrier and restriction of drug delivery to invasive glioma cells: findings in an orthotopic rat xenograft model of glioma. Drug Metab. Dispos. *41*, 33–39.

3. Kim, M., Gillies, R.J., and Rejniak, K.A. (2013). Current advances in mathematical modeling of anticancer drug penetration into tumor tissues. Front. Oncol. *3*, 278.

4. Vogelbaum, M.A., and Aghi, M.K. (2015). Convection-enhanced delivery for the treatment of glioblastoma. Neuro-oncol. *17* (*Suppl 2*), ii3–ii8.

5. Sottoriva, A., Spiteri, I., Piccirillo, S.G.M., Touloumis, A., Collins, V.P., Marioni, J.C., Curtis, C., Watts, C., and Tavaré, S. (2013). Intratumor heterogeneity in human glioblastoma reflects cancer evolutionary dynamics. Proc. Natl. Acad. Sci. USA *110*, 4009–4014.

6. Lemée, J.M., Clavreul, A., and Menei, P. (2015). Intratumoral heterogeneity in glioblastoma: don't forget the peritumoral brain zone. Neuro-oncol. *17*, 1322–1332.

7. Patel, S.J., Shapiro, W.R., Laske, D.W., Jensen, R.L., Asher, A.L., Wessels, B.W., Carpenter, S.P., and Shan, J.S. (2005). Safety and feasibility of convection-enhanced delivery of Cotara for the treatment of malignant glioma: initial experience in 51 patients. Neurosurgery *56*, 1243–1252, discussion 1252–1253.

8. Peer, D., Karp, J.M., Hong, S., Farokhzad, O.C., Margalit, R., and Langer, R. (2007). Nanocarriers as an emerging platform for cancer therapy. Nat. Nanotechnol. *2*, 751–760.

9. Min, Y., Caster, J.M., Eblan, M.J., and Wang, A.Z. (2015). Clinical translation of nanomedicine. Chem. Rev. *115*, 11147–11190.

10. Rao, W., Wang, H., Han, J., Zhao, S., Dumbleton, J., Agarwal, P., Zhang, W., Zhao, G., Yu, J., Zynger, D.L., et al. (2015). Chitosan-decorated doxorubicin-encapsulated nanoparticle targets and eliminates tumor reinitiating cancer stem-like cells. ACS Nano *9*, 5725–5740.

11. Choi, H.S., Liu, W., Misra, P., Tanaka, E., Zimmer, J.P., Itty Ipe, B., Bawendi, M.G., and Frangioni, J.V. (2007). Renal clearance of quantum dots. Nat. Biotechnol. *25*, 1165–1170.

12. Jain, R.K., and Stylianopoulos, T. (2010). Delivering nanomedicine to solid tumors. Nat. Rev. Clin. Oncol. *7*, 653–664.

13. Florence, A.T. (2012). "Targeting" nanoparticles: the constraints of physical laws and physical barriers. J. Control. Release *164*, 115–124.

14. Nichols, J.W., and Bae, Y.H. (2012). Odyssey of a cancer nanoparticle: from injection site to site of action. Nano Today *7*, 606–618.

15. Lazarovits, J., Chen, Y.Y., Sykes, E.A., and Chan, W.C.W. (2015). Nanoparticle-blood interactions: the implications on solid tumour targeting. Chem. Commun. (Camb.) *51*, 2756–2767.

16. Wilhelm, S., Tavares, A.J., Dai, Q., Ohta, S., Audet, J., Dvorak, H.F., and Chan, W.C. (2016). Analysis of nanoparticle delivery to tumours. Nat. Rev. Mater. *1*, 16014.

17. Karow, M., and Georgopoulos, C. (1992). Isolation and characterization of the *Escherichia coli msbB* gene, a multicopy suppressor of null mutations in the high-temperature requirement gene *htrB*. J. Bacteriol. *174*, 702–710.

18. Clementz, T., Zhou, Z., and Raetz, C.R. (1997). Function of the *Escherichia coli msbB* gene, a multicopy suppressor of htrB knockouts, in the acylation of lipid A. Acylation by MsbB follows laurate incorporation by HtrB. J. Biol. Chem. *272*, 10353–10360.

19. Khan, S.A., Everest, P., Servos, S., Foxwell, N., Zähringer, U., Brade, H., Rietschel, E.T., Dougan, G., Charles, I.G., and Maskell, D.J. (1998). A lethal role for lipid A in *Salmonella* infections. Mol. Microbiol. *29*, 571–579.

20. Rosenberg, S.A., Spiess, P.J., and Kleiner, D.E. (2002). Antitumor effects in mice of the intravenous injection of attenuated *Salmonella typhimurium*. J. Immunother. *25*, 218–225.

21. Low, K.B., Ittensohn, M., Luo, X., Zheng, L.M., King, I., Pawelek, J.M., and Bermudes, D. (2004). Construction of VNP20009: a novel, genetically stable antibiotic-sensitive strain of tumor-targeting *Salmonella* for parenteral administration in humans. Methods Mol. Med. *90*, 47–60.

22. Toso, J.F., Gill, V.J., Hwu, P., Marincola, F.M., Restifo, N.P., Schwartzentruber, D.J., Sherry, R.M., Topalian, S.L., Yang, J.C., Stock, F., et al. (2002). Phase I study of the intravenous administration of attenuated *Salmonella typhimurium* to patients with metastatic melanoma. J. Clin. Oncol. *20*, 142–152.

23. Low, K.B., Ittensohn, M., Le, T., Platt, J., Sodi, S., Amoss, M., Ash, O., Carmichael, E., Chakraborty, A., Fischer, J., et al. (1999). Lipid A mutant *Salmonella* with suppressed virulence and TNFalpha induction retain tumor-targeting in vivo. Nat. Biotechnol. *17*, 37–41.

24. Pawelek, J.M., Low, K.B., and Bermudes, D. (1997). Tumor-targeted *Salmonella* as a novel anticancer vector. Cancer Res. *57*, 4537–4544.

25. Buffon, A., Wink, M.R., Ribeiro, B.V., Casali, E.A., Libermann, T.A., Zerbini, L.F., Robson, S.C., and Sarkis, J.J. (2007). NTPDase and 5′ ecto-nucleotidase expression profiles and the pattern of extracellular ATP metabolism in the Walker 256 tumor. Biochim. Biophys. Acta *1770*, 1259–1265.

26. Pellegatti, P., Raffaghello, L., Bianchi, G., Piccardi, F., Pistoia, V., and Di Virgilio, F. (2008). Increased level of extracellular ATP at tumor sites: in vivo imaging with plasma membrane luciferase. PLoS One *3*, e2599.

27. Di Virgilio, F. (2012). Purines, purinergic receptors, and cancer. Cancer Res. *72*, 5441–5447.

28. Haldar, S., Negrini, M., Monne, M., Sabbioni, S., and Croce, C.M. (1994). Down-regulation of bcl-2 by p53 in breast cancer cells. Cancer Res. *54*, 2095–2097.

29. Miyashita, T., Harigai, M., Hanada, M., and Reed, J.C. (1994). Identification of a p53-dependent negative response element in the *bcl-2* gene. Cancer Res. *54*, 3131–3135.

30. Miyashita, T., and Reed, J.C. (1995). Tumor suppressor p53 is a direct transcriptional activator of the human *bax* gene. Cell *80*, 293–299.

31. Oda, E., Ohki, R., Murasawa, H., Nemoto, J., Shibue, T., Yamashita, T., Tokino, T., Taniguchi, T., and Tanaka, N. (2000). Noxa, a BH3-only member of the Bcl-2 family and candidate mediator of p53-induced apoptosis. Science *288*, 1053–1058.

32. Nakano, K., and Vousden, K.H. (2001). PUMA, a novel proapoptotic gene, is induced by p53. Mol. Cell *7*, 683–694.

33. Degli Esposti, M., and Dive, C. (2003). Mitochondrial membrane permeabilisation by Bax/Bak. Biochem. Biophys. Res. Commun. *304*, 455–461.

34. Scorrano, L., and Korsmeyer, S.J. (2003). Mechanisms of cytochrome c release by pro-apoptotic BCL-2 family members. Biochem. Biophys. Res. Commun. *304*, 437–444.

35. Sigal, A., and Rotter, V. (2000). Oncogenic mutations of the p53 tumor suppressor: the demons of the guardian of the genome. Cancer Res. *60*, 6788–6793.

36. Kim, E., and Deppert, W. (2004). Transcriptional activities of mutant p53: when mutations are more than a loss. J. Cell. Biochem. *93*, 878–886.

37. Soussi, T., Kato, S., Levy, P.P., and Ishioka, C. (2005). Reassessment of the TP53 mutation database in human disease by data mining with a library of TP53 missense mutations. Hum. Mutat. *25*, 6–17.

38. Ohgaki, H. (2005). Genetic pathways to glioblastomas. Neuropathology *25*, 1–7.

39. Nagpal, J., Jamoona, A., Gulati, N.D., Mohan, A., Braun, A., Murali, R., and Jhanwar-Uniyal, M. (2006). Revisiting the role of p53 in primary and secondary glioblastomas. Anticancer Res. *26* (6C), 4633–4639.

40. Zheleva, D.I., Lane, D.P., and Fischer, P.M. (2003). The p53-Mdm2 pathway: targets for the development of new anticancer therapeutics. Mini Rev. Med. Chem. *3*, 257–270.

41. Wang, W., Kim, S.H., and El-Deiry, W.S. (2006). Small-molecule modulators of p53 family signaling and antitumor effects in p53-deficient human colon tumor xenografts. Proc. Natl. Acad. Sci. USA *103*, 11003–11008.

42. Wiman, K.G. (2006). Strategies for therapeutic targeting of the p53 pathway in cancer. Cell Death Differ. *13*, 921–926.

43. Chaudhari, A., Mahfouz, M., Fialho, A.M., Yamada, T., Granja, A.T., Zhu, Y., Hashimoto, W., Schlarb-Ridley, B., Cho, W., Das Gupta, T.K., and Chakrabarty, A.M. (2007). Cupredoxin-cancer interrelationship: azurin binding with EphB2, interference in EphB2 tyrosine phosphorylation, and inhibition of cancer growth. Biochemistry *46*, 1799–1810.

44. Chakrabarty, A.M. (2012). Bacterial proteins: a new class of cancer therapeutics. J. Commer. Biotechnol. *18*, 4–10.

45. Chakrabarty, A.M., Bernardes, N., and Fialho, A.M. (2014). Bacterial proteins and peptides in cancer therapy: today and tomorrow. Bioengineered *5*, 234–242.

46. Maki, C.G., Huibregtse, J.M., and Howley, P.M. (1996). In vivo ubiquitination and proteasome-mediated degradation of p53(1). Cancer Res. *56*, 2649–2654.

47. Yamada, T., Goto, M., Punj, V., Zaborina, O., Chen, M.L., Kimbara, K., Majumdar, D., Cunningham, E., Das Gupta, T.K., and Chakrabarty, A.M. (2002). Bacterial redox protein azurin, tumor suppressor protein p53, and regression of cancer. Proc. Natl. Acad. Sci. USA *99*, 14098–14103.

48. Reich, N.C., and Levine, A.J. (1984). Growth regulation of a cellular tumour antigen, p53, in nontransformed cells. Nature *308*, 199–201.

49. Hong, C.S., Yamada, T., Fialho, A.M., Das Gupta, T.K., and Chakrabarty, A.M. (2006). Disrupting the entry barrier and attacking brain tumors: the role of the *Neisseria* H.8 epitope and the Laz protein. Cell Cycle *5*, 1633–1641.

50. Fialho, A.M., Salunkhe, P., Manna, S., Mahali, S., and Chakrabarty, A.M. (2012). Glioblastoma multiforme: novel therapeutic approaches. ISRN Neurol. *2012*, 642345.

51. Warso, M.A., Richards, J.M., Mehta, D., Christov, K., Schaeffer, C., Rae Bressler, L., Yamada, T., Majumdar, D., Kennedy, S.A., Beattie, C.W., and Das Gupta, T.K. (2013). A first-in-class, first-in-human, phase I trial of p28, a non-HDM2-mediated peptide inhibitor of p53 ubiquitination in patients with advanced solid tumours. Br. J. Cancer *108*, 1061–1070.

52. Leschner, S., Deyneko, I.V., Lienenklaus, S., Wolf, K., Bloecker, H., Bumann, D., Loessner, H., and Weiss, S. (2012). Identification of tumor-specific *Salmonella Typhimurium* promoters and their regulatory logic. Nucleic Acids Res. *40*, 2984–2994.

53. Arrach, N., Zhao, M., Porwollik, S., Hoffman, R.M., and McClelland, M. (2008). *Salmonella* promoters preferentially activated inside tumors. Cancer Res. *68*, 4827–4832.

54. Chorobik, P., Czaplicki, D., Ossysek, K., and Bereta, J. (2013). *Salmonella* and cancer: from pathogens to therapeutics. Acta Biochim. Pol. *60*, 285–297.

55. Stark, C., Breitkreutz, B.J., Reguly, T., Boucher, L., Breitkreutz, A., and Tyers, M. (2006). BioGRID: a general repository for interaction datasets. Nucleic Acids Res. *34*, D535–D539.

56. Kanehisa, M., Sato, Y., Kawashima, M., Furumichi, M., and Tanabe, M. (2016). KEGG as a reference resource for gene and protein annotation. Nucleic Acids Res. *44* (D1), D457–D462.

57. Wang, C.Z., Kazmierczak, R.A., and Eisenstark, A. (2016). Strains, mechanism, and perspective: *Salmonella*-based cancer therapy. Int. J. Microbiol. *2016*, 5678702.

58. Zheng, L.M., Luo, X., Feng, M., Li, Z., Le, T., Ittensohn, M., Trailsmith, M., Bermudes, D., Lin, S.L., and King, I.C. (2000). Tumor amplified protein expression therapy: *Salmonella* as a tumor-selective protein delivery vector. Oncol. Res. *12*, 127–135.

59. Chen, J., Yang, B., Cheng, X., Qiao, Y., Tang, B., Chen, G., Wei, J., Liu, X., Cheng, W., Du, P., et al. (2012). *Salmonella*-mediated tumor-targeting TRAIL gene therapy significantly suppresses melanoma growth in mouse model. Cancer Sci. *103*, 325–333.

60. Gomez-Manzano, C., Fueyo, J., Kyritsis, A.P., McDonnell, T.J., Steck, P.A., Levin, V.A., and Yung, W.K. (1997). Characterization of p53 and p21 functional interactions in glioma cells en route to apoptosis. J. Natl. Cancer Inst. *89*, 1036–1044.

61. Komata, T., Kondo, Y., Koga, S., Ko, S.C., Chung, L.W.K., and Kondo, S. (2000). Combination therapy of malignant glioma cells with 2-5A-antisense telomerase RNA and recombinant adenovirus p53. Gene Ther. *7*, 2071–2079.

62. Ito, H., Kanzawa, T., Miyoshi, T., Hirohata, S., Kyo, S., Iwamaru, A., Aoki, H., Kondo, Y., and Kondo, S. (2005). Therapeutic efficacy of PUMA for malignant glioma cells regardless of p53 status. Hum. Gene Ther. *16*, 685–698.

63. Rogers, D.E. (1960). Host mechanisms which act to remove bacteria from the blood stream. Bacteriol. Rev. *24*, 50–66.

64. Ashare, A., Stanford, C., Hancock, P., Stark, D., Lilli, K., Birrer, E., Nymon, A., Doerschug, K.C., and Hunninghake, G.W. (2009). Chronic liver disease impairs bacterial clearance in a human model of induced bacteremia. Clin. Transl. Sci. *2*, 199–205.

65. Minasyan, H. (2016). Mechanisms and pathways for the clearance of bacteria from blood circulation in health and disease. Pathophysiology *23*, 61–66.

66. Frosina, G. (2009). DNA repair and resistance of gliomas to chemotherapy and radiotherapy. Mol. Cancer Res. *7*, 989–999.

67. Bian, J., and Sun, Y. (1997). Transcriptional activation by p53 of the human type IV collagenase (gelatinase A or matrix metalloproteinase 2) promoter. Mol. Cell. Biol. *17*, 6330–6338.

68. Haar, C.P., Hebbar, P., Wallace, G.C., 4th, Das, A., Vandergrift, W.A., 3rd, Smith, J.A., Giglio, P., Patel, S.J., Ray, S.K., and Banik, N.L. (2012). Drug resistance in glioblastoma: a mini review. Neurochem. Res. *37*, 1192–1200.

69. Ma, J., Cui, W., He, S.M., Duan, Y.H., Heng, L.J., Wang, L., and Gao, G.D. (2012). Human U87 astrocytoma cell invasion induced by interaction of βig-h3 with integrin α5β1 involves calpain-2. PLoS One *7*, e37297.

70. Suk, K. (2012). Proteomic analysis of glioma chemoresistance. Curr. Neuropharmacol. *10*, 72–79.

71. Holohan, C., Van Schaeybroeck, S., Longley, D.B., and Johnston, P.G. (2013). Cancer drug resistance: an evolving paradigm. Nat. Rev. Cancer *13*, 714–726.

72. Nistico, L., Gieseke, A., Stoodley, P., Hall-Stoodley, L., Kerschner, J.E., and Ehrlich, G.D. (2009). Fluorescence "in situ" hybridization for the detection of biofilm in the middle ear and upper respiratory tract mucosa. Methods Mol. Biol. *493*, 191–213.

73. Choi, H., Fermin, D., and Nesvizhskii, A.I. (2008). Significance analysis of spectral count data in label-free shotgun proteomics. Mol. Cell. Proteomics *7*, 2373–2385.

74. Reimand, J., Arak, T., and Vilo, J. (2011). g:Profiler—a web server for functional interpretation of gene lists (2011 update). Nucleic Acids Res. *39*, W307–W315.

75. Subramanian, A., Tamayo, P., Mootha, V.K., Mukherjee, S., Ebert, B.L., Gillette, M.A., Paulovich, A., Pomeroy, S.L., Golub, T.R., Lander, E.S., and Mesirov, J.P. (2005). Gene set enrichment analysis: a knowledge-based approach for interpreting genome-wide expression profiles. Proc. Natl. Acad. Sci. USA *102*, 15545–15550.

76. Merico, D., Isserlin, R., Stueker, O., Emili, A., and Bader, G.D. (2010). Enrichment map: a network-based method for gene-set enrichment visualization and interpretation. PLoS One *5*, e13984.

77. Shannon, P., Markiel, A., Ozier, O., Baliga, N.S., Wang, J.T., Ramage, D., Amin, N., Schwikowski, B., and Ideker, T. (2003). Cytoscape: a software environment for integrated models of biomolecular interaction networks. Genome Res. *13*, 2498–2504.

OMTO, Volume *4*

Supplemental Information

Bacterial Carriers for Glioblastoma Therapy

Nalini Mehta, Johnathan G. Lyon, Ketki Patil, Nassir Mokarram, Christine Kim, and Ravi V. Bellamkonda

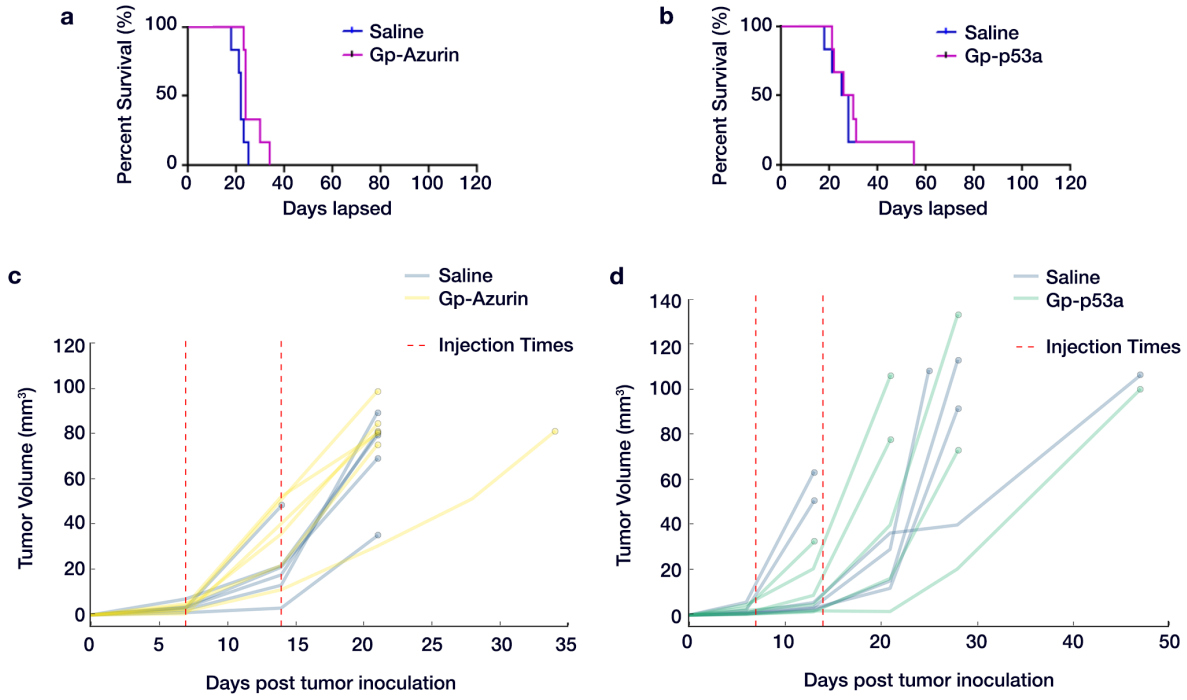

Supplemental Figure S1. Kaplan Meier plot for control (n =6 for each set) and treated rats that were injected with carrier expressing either **(a)** Azurin (n = 6) or **(b)** p53, (n = 6). Results showed no survival in control and treated rat group. *p* value = 0.0263 for Azurin survival plot and *p* value = 0.6721 for p53 survival plot. **(c)** Tumor volumes calculated from MRI images for control (n = 6) and carrier treated rats expressing *only Azurin* (n = 6). Tumor volume increased exponentially in all control and treated rats. **(d)** Tumor volumes calculated from MRI images for control (n = 6) and carrier treated rats expressing *only p53* (n = 6). Tumor volume increased exponentially in all control and treated rats.

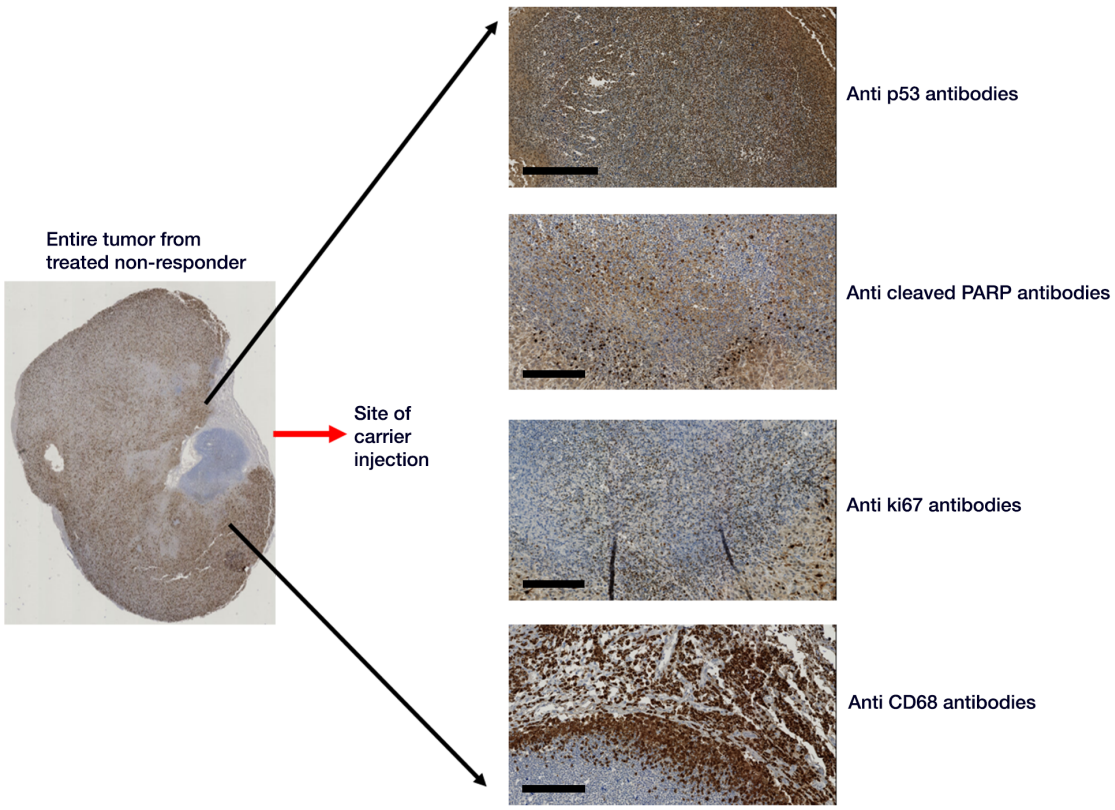

Supplement Figure S2. Multiple responses to apoptotic proteins are observed following carrier injection. Near the site of carrier injection, there is increased expression of p53, increase in cleaved PARP (indicator of apoptosis), decrease in ki67 (indicator for cell proliferation), and an increased influx of activated microglia or CD68 positive cells (indicator of innate immune response). In spite of multiple responses, the tumor of non-responders continued to grow possibly because the rate of tumor proliferation exceeded the rate of apoptosis. Picture shown on left is entire tumor from a non-responder rat stained with anti-ki67 antibodies showing high proliferation rate in most part of the tumor except the site of carrier injection. Scale bars: 200 μm.

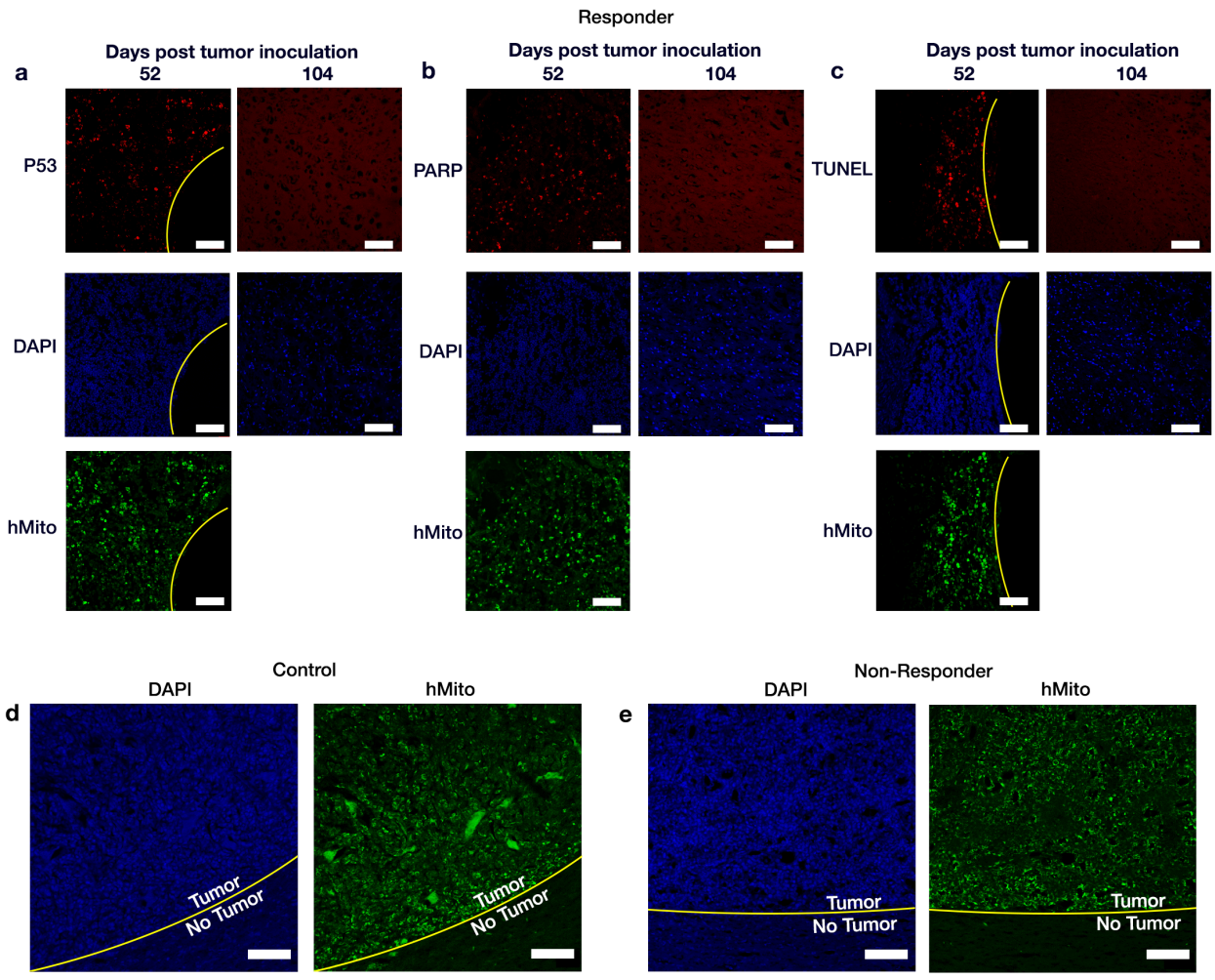

Supplemental Figure S3. IHC images of brain sections from treated responder rats euthanized on day 52 post tumor implant or at day 104 to check for presence of **(a)** p53, **(b)** PARP, or **(c)** TUNEL, each stained red above. Green- human anti-mitochondria antibodies which specifically stains tumor cells, Blue-DAPI. The sections show sparsely dispersed tumor cells (green) on day 52. Right side of yellow line - carrier injection site shows a big gap, presumably the site where tumor cells were originally proliferating. In the 52-day section, lot of p53, PARP and TUNEL staining observed exclusively within tumor region. The adjacent healthy cells did not show TUNEL staining indicating absence of apoptosis in this region. In the day 104 sections, p53, PARP and TUNEL staining was negative. There were no glioma cells in all of the responder tissues euthanized on day 104 (**See Fig 6a**), thus no representative human anti-mitochondrial signal for these conditions. Compared to treated responder rats, the tumor population from **(d)** control and **(e)** treated non-responder rats was dense**.** Yellow lines demarcate intra- and extra-tumoral regions. Scale bars: 100 μm.

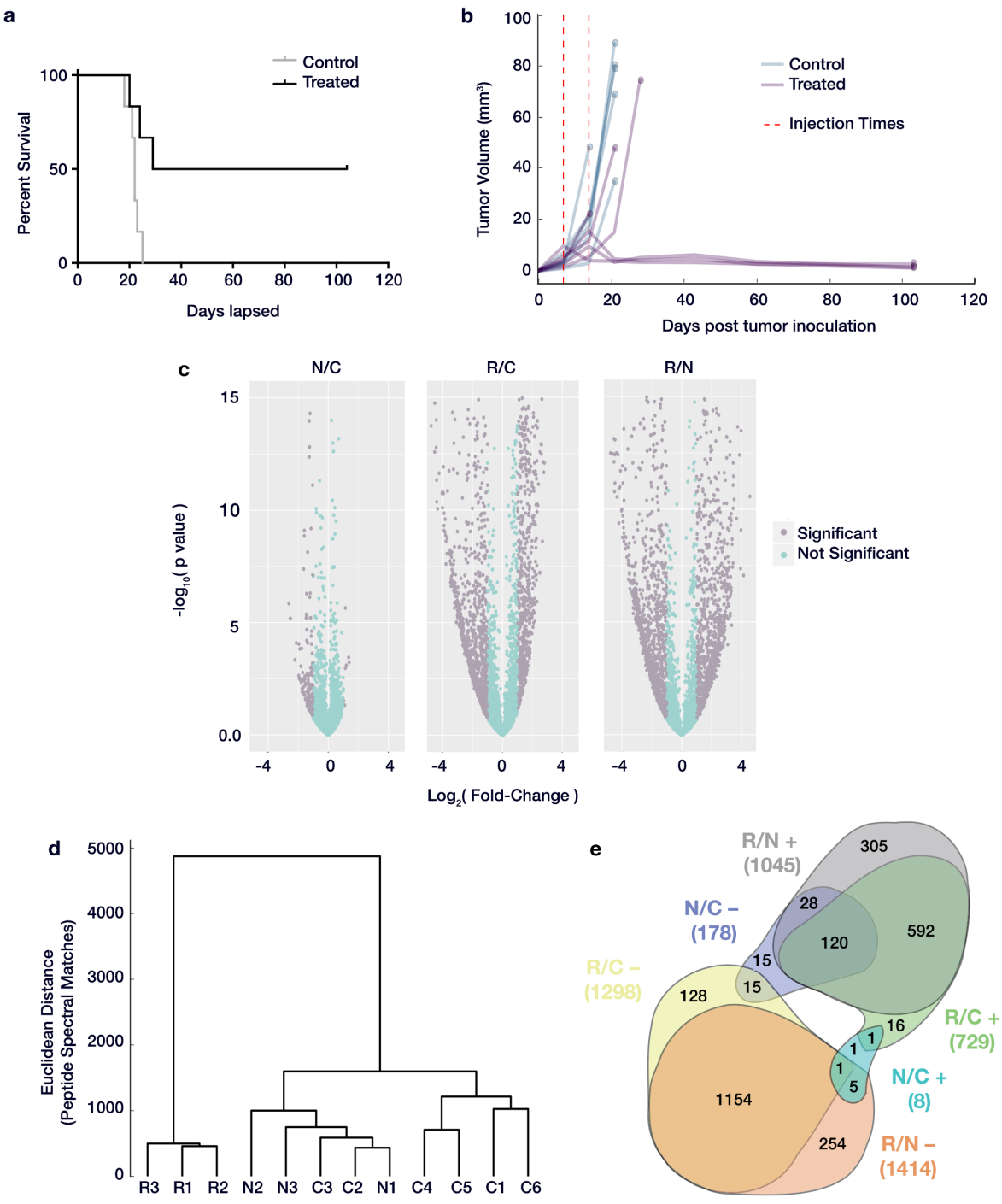

Supplemental Figure S4. (a) Survival analysis and **(b)** tumor volumes for animal cohort used in proteomic analysis (12 animals, 6 control, 3 non-responder, 3 responder). **(C)** Volcano plots depicting significantly differentially expressed proteins. Each dot represents a unique protein (by uniprot accession). Significant threshold was set to a false discovery rate of < 0.05 and a fold change of greater than ±2-fold. (d) Dendrogram

clustering of proteomics samples by Euclidian distance between peptide spectrum matches across all measured proteins. Note the strong clustering of responders (R1-3), while the non-responders (N1-3) and controls (C1-6) are more closely related in their proteomic signature. **(e)** Euler Diagram depicting overlapping membership of differentially expressed proteins across the fold-change pairs and further subset by whether this differential expression was relatively an up- or down- fold change. Numbers in parentheses indicate total number of proteins in that particular differential expression subset. R/C is differentially expressed proteins in responders relative to controls, N/C is non-responders relative to controls, and R/N is responders relative to controls, where the sign indicates either +: up- or –: down- fold differential expression.

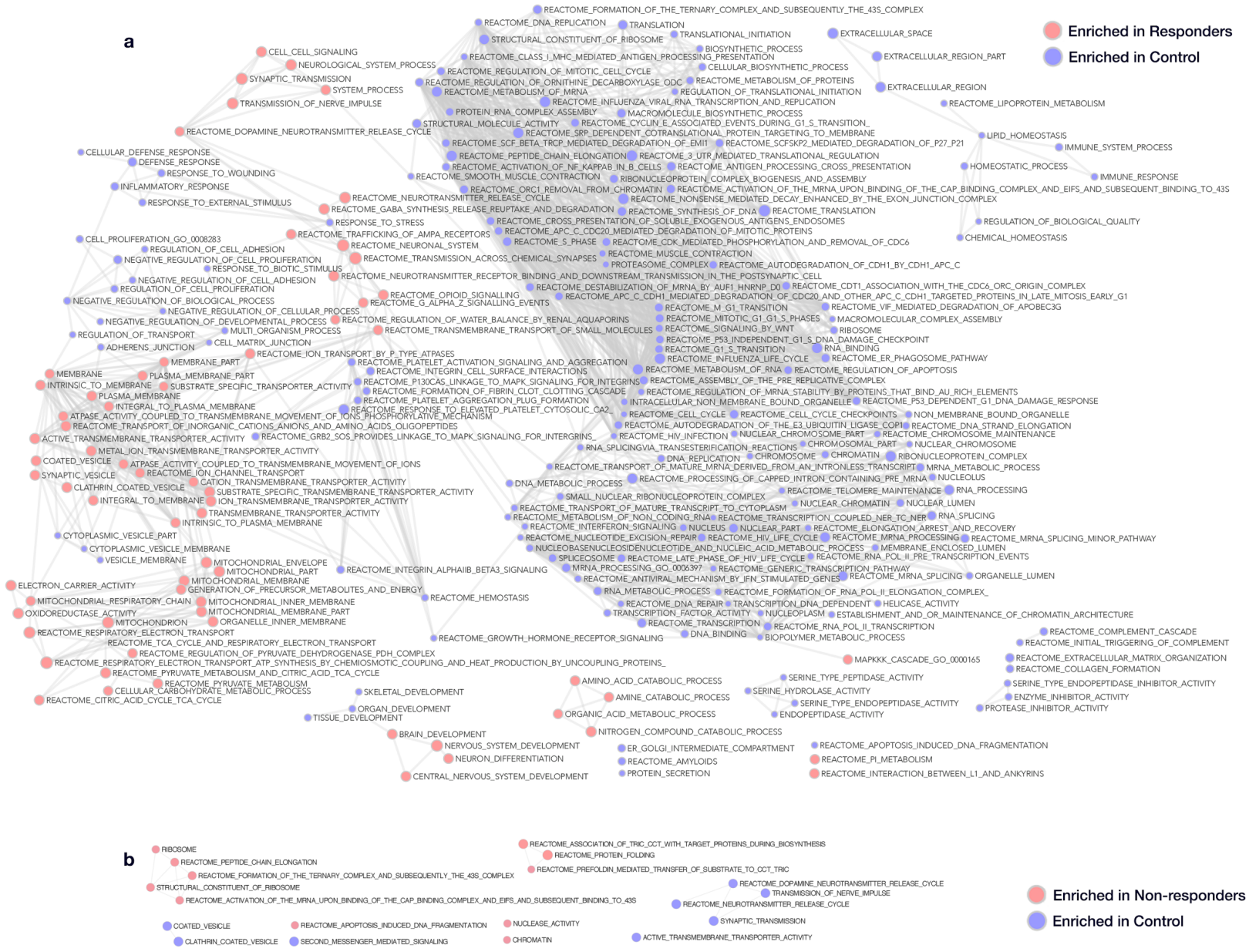
a
Enriched in Responders
Enriched in Control
REACTOME_FORMATION_OF_THE_TERNARY_COMPLEX_AND_SUBSEQUENTLY_THE_43S_COMPLEX
REACTOME_DNA_REPLICATION
TRANSLATION
TRANSLATIONAL_INITIATION
EXTRACELLULAR_SPACE
STRUCTURAL_CONSTITUENT_OF_RIBOSOME
CELL_CELL_SIGNALING
BIOSYNTHETIC_PROCESS
NEUROLOGICAL_SYSTEM_PROCESS
REACTOME_CLASS_I_MHC_MEDIATED_ANTIGEN_PROCESSING_PRESENTATION
EXTRACELLULAR_REGION_PART
SYNAPTIC_TRANSMISSION
REACTOME_REGULATION_OF_MITOTIC_CELL_CYCLE
CELLULAR_BIOSYNTHETIC_PROCESS
SYSTEM_PROCESS
REACTOME_REGULATION_OF_ORNITHINE_DECARBOXYLASE_ODC
REACTOME_METABOLISM_OF_PROTEINS
EXTRACELLULAR_REGION
REACTOME_METABOLISM_OF_MRNA
REGULATION_OF_TRANSLATIONAL_INITIATION
TRANSMISSION_OF_NERVE_IMPULSE
REACTOME_INFLUENZA_VIRAL_RNA_TRANSCRIPTION_AND_REPLICATION
REACTOME_LIPOPROTEIN_METABOLISM
PROTEIN_RNA_COMPLEX_ASSEMBLY
MACROMOLECULE_BIOSYNTHETIC_PROCESS
STRUCTURAL_MOLECULE_ACTIVITY
REACTOME_CYCLIN_E_ASSOCIATED_EVENTS_DURING_G1_S_TRANSITION_
REACTOME_DOPAMINE_NEUROTRANSMITTER_RELEASE_CYCLE
REACTOME_SRP_DEPENDENT_COTRANSLATIONAL_PROTEIN_TARGETING_TO_MEMBRANE
LIPID_HOMEOSTASIS
REACTOME_SCF_BETA_TRCP_MEDIATED_DEGRADATION_OF_EMI1
REACTOME_SCFSKP2_MEDIATED_DEGRADATION_OF_P27_P21
IMMUNE_SYSTEM_PROCESS
CELLULAR_DEFENSE_RESPONSE
REACTOME_PEPTIDE_CHAIN_ELONGATION
REACTOME_3_UTR_MEDIATED_TRANSLATIONAL_REGULATION
DEFENSE_RESPONSE
REACTOME_ACTIVATION_OF_NF_KAPPAB_IN_B_CELLS
REACTOME_ANTIGEN_PROCESSING_CROSS_PRESENTATION
HOMEOSTATIC_PROCESS
RESPONSE_TO_WOUNDING
REACTOME_SMOOTH_MUSCLE_CONTRACTION
RIBONUCLEOPROTEIN_COMPLEX_BIOGENESIS_AND_ASSEMBLY
IMMUNE_RESPONSE
INFLAMMATORY_RESPONSE
REACTOME_ORC1_REMOVAL_FROM_CHROMATIN
REACTOME_ACTIVATION_OF_THE_MRNA_UPON_BINDING_OF_THE_CAP_BINDING_COMPLEX_AND_EIFS_AND_SUBSEQUENT_BINDING_TO_43S
REACTOME_NEUROTRANSMITTER_RELEASE_CYCLE
REACTOME_NONSENSE_MEDIATED_DECAY_ENHANCED_BY_THE_EXON_JUNCTION_COMPLEX
RESPONSE_TO_EXTERNAL_STIMULUS
REACTOME_GABA_SYNTHESIS_RELEASE_REUPTAKE_AND_DEGRADATION
REACTOME_SYNTHESIS_OF_DNA
REACTOME_TRANSLATION
REACTOME_CROSS_PRESENTATION_OF_SOLUBLE_EXOGENOUS_ANTIGENS_ENDOSOMES
REGULATION_OF_BIOLOGICAL_QUALITY
RESPONSE_TO_STRESS
REACTOME_APC_C_CDC20_MEDIATED_DEGRADATION_OF_MITOTIC_PROTEINS
REACTOME_TRAFFICKING_OF_AMPA_RECEPTORS
CHEMICAL_HOMEOSTASIS
CELL_PROLIFERATION_GO_0008283
REACTOME_S_PHASE
REACTOME_CDK_MEDIATED_PHOSPHORYLATION_AND_REMOVAL_OF_CDC6
REGULATION_OF_CELL_ADHESION
REACTOME_NEURONAL_SYSTEM
REACTOME_MUSCLE_CONTRACTION
NEGATIVE_REGULATION_OF_CELL_PROLIFERATION
REACTOME_TRANSMISSION_ACROSS_CHEMICAL_SYNAPSES
PROTEASOME_COMPLEX
REACTOME_AUTODEGRADATION_OF_CDH1_BY_CDH1_APC_C
RESPONSE_TO_BIOTIC_STIMULUS
REACTOME_NEUROTRANSMITTER_RECEPTOR_BINDING_AND_DOWNSTREAM_TRANSMISSION_IN_THE_POSTSYNAPTIC_CELL
NEGATIVE_REGULATION_OF_CELL_ADHESION
REACTOME_DESTABILIZATION_OF_MRNA_BY_AUF1_HNRNP_D0
REACTOME_CDT1_ASSOCIATION_WITH_THE_CDC6_ORC_ORIGIN_COMPLEX
REGULATION_OF_CELL_PROLIFERATION
REACTOME_OPIOID_SIGNALLING
REACTOME_APC_C_CDH1_MEDIATED_DEGRADATION_OF_CDC20_AND_OTHER_APC_C_CDH1_TARGETED_PROTEINS_IN_LATE_MITOSIS_EARLY_G1
NEGATIVE_REGULATION_OF_BIOLOGICAL_PROCESS
REACTOME_G_ALPHA_Z_SIGNALLING_EVENTS
REACTOME_M_G1_TRANSITION
REACTOME_VIF_MEDIATED_DEGRADATION_OF_APOBEC3G
NEGATIVE_REGULATION_OF_CELLULAR_PROCESS
NEGATIVE_REGULATION_OF_DEVELOPMENTAL_PROCESS
REACTOME_REGULATION_OF_WATER_BALANCE_BY_RENAL_AQUAPORINS
REACTOME_MITOTIC_G1_G1_S_PHASES
MACROMOLECULAR_COMPLEX_ASSEMBLY
REGULATION_OF_TRANSPORT
MULTI_ORGANISM_PROCESS
REACTOME_TRANSMEMBRANE_TRANSPORT_OF_SMALL_MOLECULES
REACTOME_SIGNALING_BY_WNT
RIBOSOME
ADHERENS_JUNCTION
CELL_MATRIX_JUNCTION
REACTOME_P53_INDEPENDENT_G1_S_DNA_DAMAGE_CHECKPOINT
REACTOME_G1_S_TRANSITION
RNA_BINDING
REACTOME_ION_TRANSPORT_BY_P_TYPE_ATPASES
REACTOME_INFLUENZA_LIFE_CYCLE
REACTOME_ER_PHAGOSOME_PATHWAY
MEMBRANE_PART
REACTOME_PLATELET_ACTIVATION_SIGNALING_AND_AGGREGATION
MEMBRANE
PLASMA_MEMBRANE_PART
REACTOME_INTEGRIN_CELL_SURFACE_INTERACTIONS
REACTOME_METABOLISM_OF_RNA
REACTOME_REGULATION_OF_APOPTOSIS
INTRINSIC_TO_MEMBRANE
SUBSTRATE_SPECIFIC_TRANSPORTER_ACTIVITY
REACTOME_P130CAS_LINKAGE_TO_MAPK_SIGNALING_FOR_INTEGRINS
REACTOME_ASSEMBLY_OF_THE_PRE_REPLICATIVE_COMPLEX
PLASMA_MEMBRANE
REACTOME_FORMATION_OF_FIBRIN_CLOT_CLOTTING_CASCADE
REACTOME_REGULATION_OF_MRNA_STABILITY_BY_PROTEINS_THAT_BIND_AU_RICH_ELEMENTS
INTEGRAL_TO_PLASMA_MEMBRANE
REACTOME_PLATELET_AGGREGATION_PLUG_FORMATION
INTRACELLULAR_NON_MEMBRANE_BOUND_ORGANELLE
REACTOME_P53_DEPENDENT_G1_DNA_DAMAGE_RESPONSE
ATPASE_ACTIVITY_COUPLED_TO_TRANSMEMBRANE_MOVEMENT_OF_IONS_PHOSPHORYLATIVE_MECHANISM
REACTOME_RESPONSE_TO_ELEVATED_PLATELET_CYTOSOLIC_CA2_
REACTOME_CELL_CYCLE
REACTOME_CELL_CYCLE_CHECKPOINTS
NON_MEMBRANE_BOUND_ORGANELLE
REACTOME_TRANSPORT_OF_INORGANIC_CATIONS_ANIONS_AND_AMINO_ACIDS_OLIGOPEPTIDES
REACTOME_AUTODEGRADATION_OF_THE_E3_UBIQUITIN_LIGASE_COP1
REACTOME_DNA_STRAND_ELONGATION
ACTIVE_TRANSMEMBRANE_TRANSPORTER_ACTIVITY
REACTOME_GRB2_SOS_PROVIDES_LINKAGE_TO_MAPK_SIGNALING_FOR_INTERGRINS_
REACTOME_HIV_INFECTION
NUCLEAR_CHROMOSOME_PART
REACTOME_CHROMOSOME_MAINTENANCE
METAL_ION_TRANSMEMBRANE_TRANSPORTER_ACTIVITY
RNA_SPLICINGVIA_TRANSESTERIFICATION_REACTIONS
CHROMOSOMAL_PART
NUCLEAR_CHROMOSOME
COATED_VESICLE
ATPASE_ACTIVITY_COUPLED_TO_TRANSMEMBRANE_MOVEMENT_OF_IONS
DNA_REPLICATION
CHROMOSOME
CHROMATIN
RIBONUCLEOPROTEIN_COMPLEX
SYNAPTIC_VESICLE
REACTOME_ION_CHANNEL_TRANSPORT
REACTOME_TRANSPORT_OF_MATURE_MRNA_DERIVED_FROM_AN_INTRONLESS_TRANSCRIPT
MRNA_METABOLIC_PROCESS
CLATHRIN_COATED_VESICLE
CATION_TRANSMEMBRANE_TRANSPORTER_ACTIVITY
DNA_METABOLIC_PROCESS
REACTOME_PROCESSING_OF_CAPPED_INTRON_CONTAINING_PRE_MRNA
NUCLEOLUS
SUBSTRATE_SPECIFIC_TRANSMEMBRANE_TRANSPORTER_ACTIVITY
REACTOME_TELOMERE_MAINTENANCE
RNA_PROCESSING
INTEGRAL_TO_MEMBRANE
ION_TRANSMEMBRANE_TRANSPORTER_ACTIVITY
SMALL_NUCLEAR_RIBONUCLEOPROTEIN_COMPLEX
NUCLEAR_CHROMATIN
NUCLEAR_LUMEN
TRANSMEMBRANE_TRANSPORTER_ACTIVITY
REACTOME_TRANSPORT_OF_MATURE_TRANSCRIPT_TO_CYTOPLASM
INTRINSIC_TO_PLASMA_MEMBRANE
REACTOME_METABOLISM_OF_NON_CODING_RNA
REACTOME_TRANSCRIPTION_COUPLED_NER_TC_NER
RNA_SPLICING
CYTOPLASMIC_VESICLE_PART
REACTOME_INTERFERON_SIGNALING
NUCLEUS
NUCLEAR_PART
REACTOME_ELONGATION_ARREST_AND_RECOVERY
CYTOPLASMIC_VESICLE_MEMBRANE
REACTOME_NUCLEOTIDE_EXCISION_REPAIR
REACTOME_HIV_LIFE_CYCLE
REACTOME_MRNA_PROCESSING
REACTOME_MRNA_SPLICING_MINOR_PATHWAY
VESICLE_MEMBRANE
NUCLEOBASENUCLEOSIDENUCLEOTIDE_AND_NUCLEIC_ACID_METABOLIC_PROCESS
MEMBRANE_ENCLOSED_LUMEN
MITOCHONDRIAL_ENVELOPE
SPLICEOSOME
REACTOME_LATE_PHASE_OF_HIV_LIFE_CYCLE
REACTOME_RNA_POL_II_PRE_TRANSCRIPTION_EVENTS
MITOCHONDRIAL_PART
REACTOME_INTEGRIN_ALPHAIIB_BETA3_SIGNALING
MRNA_PROCESSING_GO_0006397
REACTOME_GENERIC_TRANSCRIPTION_PATHWAY
ELECTRON_CARRIER_ACTIVITY
MITOCHONDRIAL_MEMBRANE
REACTOME_ANTIVIRAL_MECHANISM_BY_IFN_STIMULATED_GENES
REACTOME_MRNA_SPLICING
ORGANELLE_LUMEN
GENERATION_OF_PRECURSOR_METABOLITES_AND_ENERGY
REACTOME_HEMOSTASIS
RNA_METABOLIC_PROCESS
REACTOME_FORMATION_OF_RNA_POL_II_ELONGATION_COMPLEX_
MITOCHONDRIAL_RESPIRATORY_CHAIN
MITOCHONDRIAL_INNER_MEMBRANE
REACTOME_DNA_REPAIR
TRANSCRIPTION_DNA_DEPENDENT
HELICASE_ACTIVITY
OXIDOREDUCTASE_ACTIVITY
MITOCHONDRIAL_MEMBRANE_PART
TRANSCRIPTION_FACTOR_ACTIVITY
NUCLEOPLASM
ESTABLISHMENT_AND_OR_MAINTENANCE_OF_CHROMATIN_ARCHITECTURE
MITOCHONDRION
ORGANELLE_INNER_MEMBRANE
REACTOME_TRANSCRIPTION
REACTOME_RNA_POL_II_TRANSCRIPTION
REACTOME_RESPIRATORY_ELECTRON_TRANSPORT
DNA_BINDING
BIOPOLYMER_METABOLIC_PROCESS
REACTOME_COMPLEMENT_CASCADE
REACTOME_GROWTH_HORMONE_RECEPTOR_SIGNALING
REACTOME_INITIAL_TRIGGERING_OF_COMPLEMENT
REACTOME_TCA_CYCLE_AND_RESPIRATORY_ELECTRON_TRANSPORT
MAPKKK_CASCADE_GO_0000165
REACTOME_EXTRACELLULAR_MATRIX_ORGANIZATION
REACTOME_REGULATION_OF_PYRUVATE_DEHYDROGENASE_PDH_COMPLEX
REACTOME_COLLAGEN_FORMATION
REACTOME_RESPIRATORY_ELECTRON_TRANSPORT_ATP_SYNTHESIS_BY_CHEMIOSMOTIC_COUPLING_AND_HEAT_PRODUCTION_BY_UNCOUPLING_PROTEINS_
AMINO_ACID_CATABOLIC_PROCESS
SERINE_TYPE_PEPTIDASE_ACTIVITY
SERINE_TYPE_ENDOPEPTIDASE_INHIBITOR_ACTIVITY
REACTOME_PYRUVATE_PYRUVATE_METABOLISM_AND_CITRIC_ACID_TCA_CYCLE
SERINE_HYDROLASE_ACTIVITY
ENZYME_INHIBITOR_ACTIVITY
REACTOME_PYRUVATE_METABOLISM
AMINE_CATABOLIC_PROCESS
SERINE_TYPE_ENDOPEPTIDASE_ACTIVITY
PROTEASE_INHIBITOR_ACTIVITY
CELLULAR_CARBOHYDRATE_METABOLIC_PROCESS
SKELETAL_DEVELOPMENT
ORGANIC_ACID_METABOLIC_PROCESS
ENDOPEPTIDASE_ACTIVITY
REACTOME_CITRIC_ACID_CYCLE_TCA_CYCLE
ORGAN_DEVELOPMENT
NITROGEN_COMPOUND_CATABOLIC_PROCESS
TISSUE_DEVELOPMENT
BRAIN_DEVELOPMENT
ER_GOLGI_INTERMEDIATE_COMPARTMENT
REACTOME_APOPTOSIS_INDUCED_DNA_FRAGMENTATION
NERVOUS_SYSTEM_DEVELOPMENT
REACTOME_AMYLOIDS
REACTOME_PI_METABOLISM
NEURON_DIFFERENTIATION
PROTEIN_SECRETION
REACTOME_INTERACTION_BETWEEN_L1_AND_ANKYRINS
CENTRAL_NERVOUS_SYSTEM_DEVELOPMENT
b
Enriched in Non-responders
Enriched in Control
RIBOSOME
REACTOME_ASSOCIATION_OF_TRIC_CCT_WITH_TARGET_PROTEINS_DURING_BIOSYNTHESIS
REACTOME_PEPTIDE_CHAIN_ELONGATION
REACTOME_PROTEIN_FOLDING
REACTOME_FORMATION_OF_THE_TERNARY_COMPLEX_AND_SUBSEQUENTLY_THE_43S_COMPLEX
REACTOME_PREFOLDIN_MEDIATED_TRANSFER_OF_SUBSTRATE_TO_CCT_TRIC
REACTOME_DOPAMINE_NEUROTRANSMITTER_RELEASE_CYCLE
STRUCTURAL_CONSTITUENT_OF_RIBOSOME
TRANSMISSION_OF_NERVE_IMPULSE
REACTOME_ACTIVATION_OF_THE_MRNA_UPON_BINDING_OF_THE_CAP_BINDING_COMPLEX_AND_EIFS_AND_SUBSEQUENT_BINDING_TO_43S
REACTOME_NEUROTRANSMITTER_RELEASE_CYCLE
SYNAPTIC_TRANSMISSION
COATED_VESICLE
REACTOME_APOPTOSIS_INDUCED_DNA_FRAGMENTATION
NUCLEASE_ACTIVITY
CLATHRIN_COATED_VESICLE
SECOND_MESSENGER_MEDIATED_SIGNALING
CHROMATIN
ACTIVE_TRANSMEMBRANE_TRANSPORTER_ACTIVITY

Supplemental Figure S5. GSEA enrichment map for significantly affected pathways (p-value < 0.05, false discovery rate < 25%) in **(A)** responders relative to controls, and **(B)** non-responders relative to control using the Reactome and Gene Ontology datasets. Red dots indicate positively enriched pathways; blue indicates negatively enriched pathways. Relative size maps to relative magnitude of Normalized enrichment score. Edge size corresponds to number of proteins that overlap between gene sets.

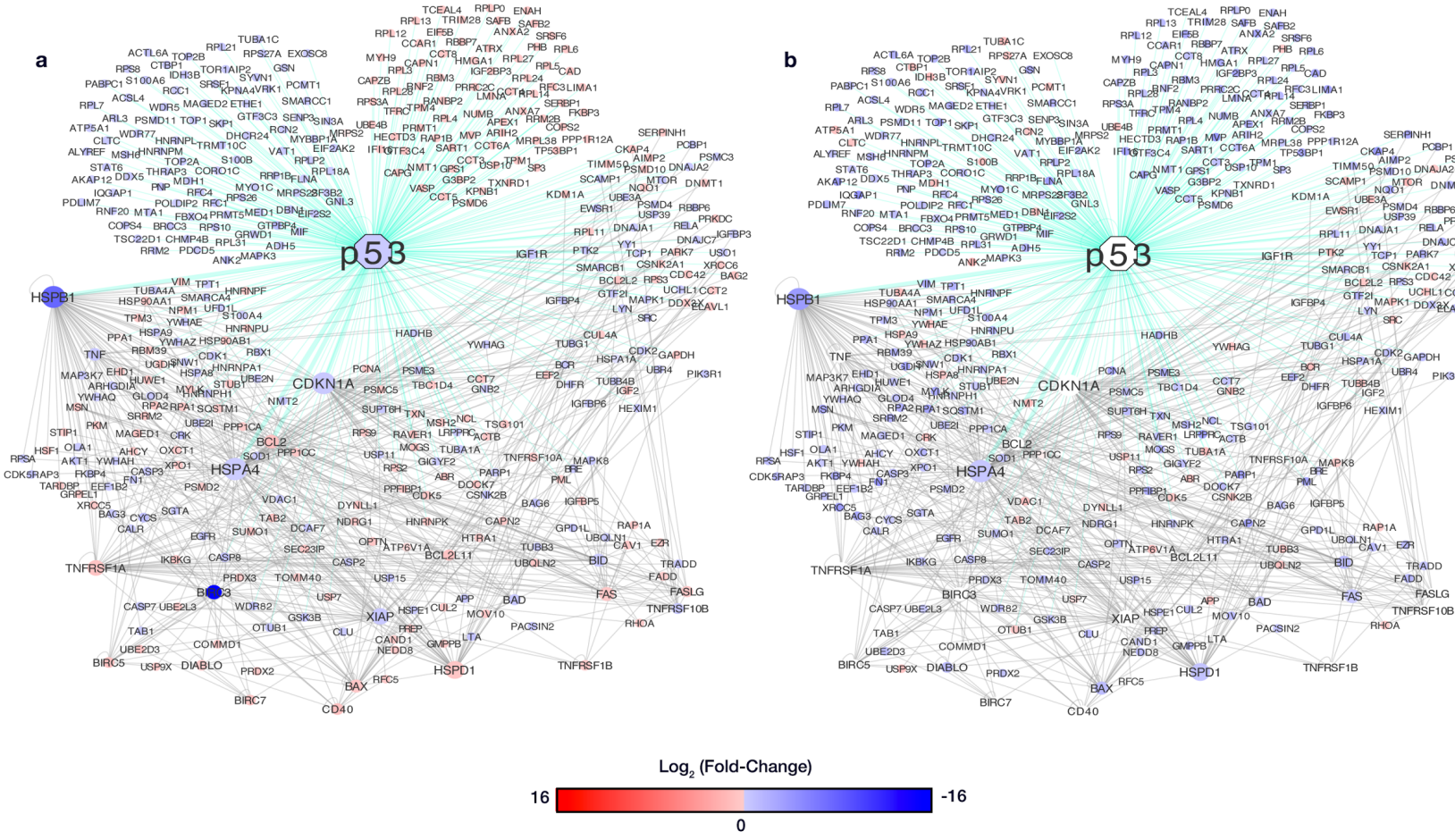
a
b
p53
HSPB1
CDKN1A
HSPA4
BCL2
BIRC3
TNFRSF1A
HSPD1
BAX
CD40
XIAP
BID
FAS
FASLG
TNFRSF10B
TNFRSF1B
Log2 (Fold-Change)
16
0
-16

Supplemental Figure S6. Gene neighborhood network (via BIOGRID and g:profiler) using proteins from apoptosis antibody array. Coloring indicated average protein fold-change for **(a)** non-responders, and **(b)** responders relative to controls using proteomics and western array data. Network has been pruned for visualization for any undetected/unmeasured protein and any node of degree 1 that was not directly connected to p53. Overall this network in non-responders is mixed in regulation, while the responder network is primarily down-regulated relative to controls.

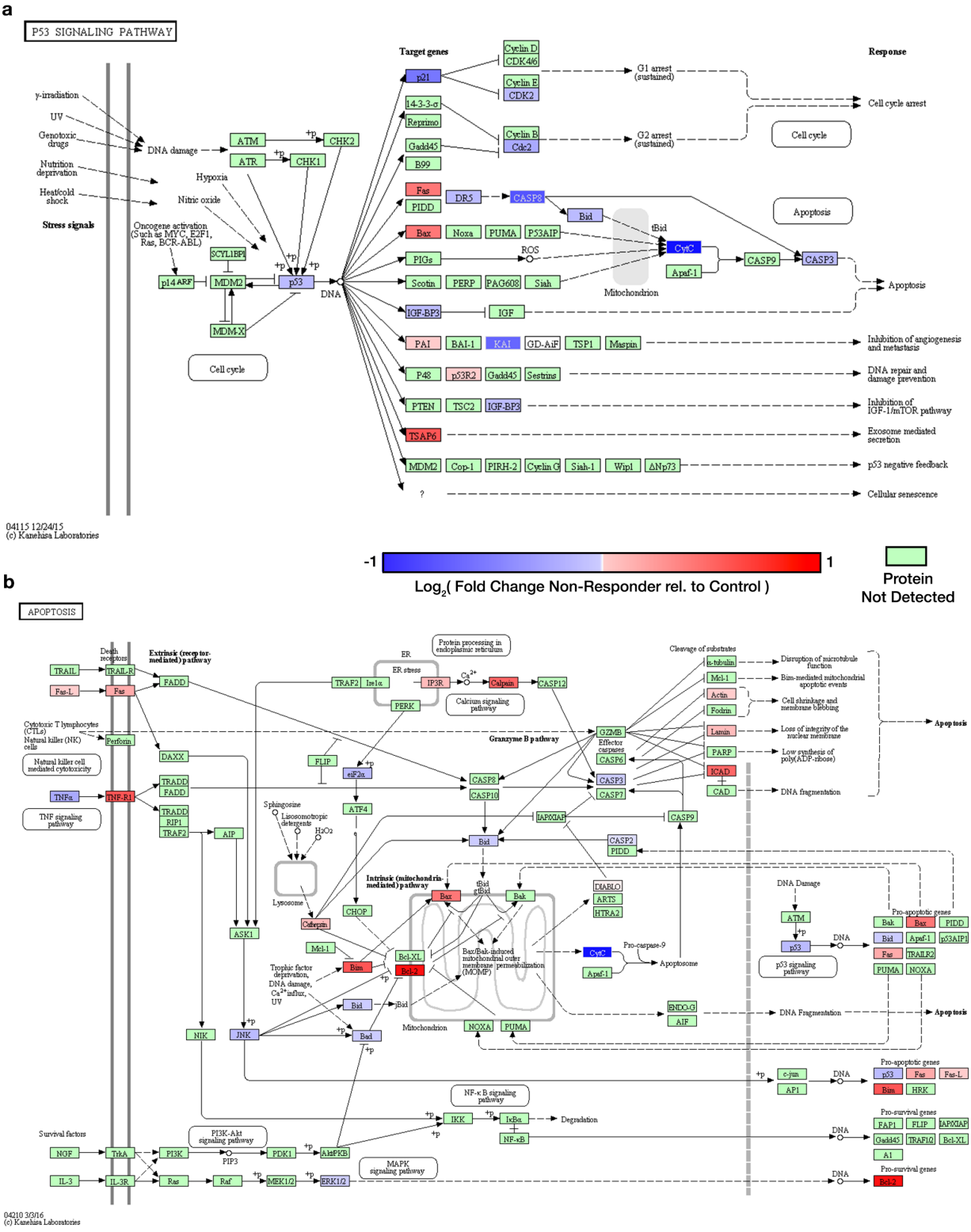
a
P53 SIGNALING PATHWAY
Target genes
Response
Stress signals
DNA damage
Hypoxia
Nitric oxide
Oncogene activation (Such as MYC, E2F1, Ras, BCR-ABL)
Heat/cold shock
Nutrition deprivation
Genotoxic drugs
UV
γ-irradiation
ATM
ATR
CHK2
CHK1
SCYL1BP1
p14 ARF
MDM2
MDM-X
p53
DNA
Cell cycle
p21
14-3-3-σ
Reprimo
Gadd45
B99
Cyclin D
CDK4/6
Cyclin E
CDK2
Cyclin B
Cdc2
G1 arrest (sustained)
G2 arrest (sustained)
Cell cycle arrest
Cell cycle
Fas
PIDD
DR5
CASP8
Bid
tBid
Bax
Noxa
PUMA
P53AIP
PIGs
ROS
Scotin
PERP
PAG608
Siah
CytC
Apaf-1
CASP9
CASP3
Mitochondrion
Apoptosis
Apoptosis
IGF-BP3
IGF
PAI
BAI-1
KAI
GD-AiF
TSP1
Maspin
Inhibition of angiogenesis and metastasis
P48
p53R2
Gadd45
Sestrins
DNA repair and damage prevention
PTEN
TSC2
IGF-BP3
Inhibition of IGF-1/mTOR pathway
TSAP6
Exosome mediated secretion
MDM2
Cop-1
PIRH-2
Cyclin G
Siah-1
Wip1
ΔNp73
p53 negative feedback
?
Cellular senescence
04115 12/24/15
(c) Kanehisa Laboratories
-1
1
Log2(Fold Change Non-Responder rel. to Control)
Protein Not Detected
b
APOPTOSIS
Death receptors
Extrinsic (receptor-mediated) pathway
TRAIL
Fas-L
TRAIL-R
Fas
FADD
Cytotoxic T lymphocytes (CTLs)
Natural killer (NK) cells
Perforin
Natural killer cell mediated cytotoxicity
TNFα
TNF-R1
TNF signaling pathway
DAXX
TRADD
FADD
TRADD
RIP1
TRAF2
AIP
ASK1
NIK
JNK
ER
Protein processing in endoplasmic reticulum
ER stress
TRAF2
Ire1α
IP3R
Ca2+
Calpain
CASP12
PERK
Calcium signaling pathway
FLIP
eIF2α
CASP8
CASP10
ATF4
Sphingosine
Lysosomotropic detergents
H2O2
Lysosome
Cathepsin
CHOP
Granzyme B pathway
GZMB
Effector caspases
CASP6
CASP3
CASP7
IAP/XIAP
CASP9
CASP2
PIDD
Bid
Intrinsic (mitochondria-mediated) pathway
Bax
tBid
Bak
DIABLO
ARTS
HTRA2
Mcl-1
Bcl-XL
Bcl-2
Bim
Trophic factor deprivation, DNA damage, Ca2+ influx, UV
Bid
jBid
Bad
Bax/Bak-induced mitochondrial outer membrane permeabilization (MOMP)
Mitochondrion
NOXA
PUMA
CytC
Apaf-1
Pro-caspase-9
Apoptosome
ENDO-G
AIF
Cleavage of substrates
α-tubulin
Mcl-1
Actin
Fodrin
Lamin
PARP
ICAD
CAD
Disruption of microtubule function
Bim-mediated mitochondrial apoptotic events
Cell shrinkage and membrane blebbing
Loss of integrity of the nuclear membrane
Low synthesis of poly(ADP-ribose)
DNA fragmentation
Apoptosis
DNA Fragmentation
Apoptosis
DNA Damage
ATM
p53
p53 signaling pathway
DNA
Pro-apoptotic genes
Bak
Bax
PIDD
Bid
Apaf-1
p53AIP1
Fas
TRAILR2
PUMA
NOXA
c-jun
AP1
DNA
Pro-apoptotic genes
p53
Fas
Fas-L
Bim
HRK
NF-κB signaling pathway
IKK
IκBα
Degradation
NF-κB
DNA
Pro-survival genes
FAP1
FLIP
IAP/XIAP
Gadd45
TRAF1/2
Bcl-XL
A1
Survival factors
NGF
TrkA
PI3K
PIP3
PDK1
Akt/PKB
PI3K-Akt signaling pathway
IL-3
IL-3R
Ras
Raf
MEK1/2
ERK1/2
MAPK signaling pathway
DNA
Pro-survival genes
Bcl-2
04210 3/3/16
(c) Kanehisa Laboratories

Supplemental Figure S7. KEGG **(a)** P53 Signaling (HAS:04115) and **(b)** Apoptosis (HSA:04210) pathways, colored using average non-responder fold-change relative to controls, using proteomics and western array data. No clear pro- or anti-apoptotic signal is apparent from these mappings i.e., both relatively positive and negative expression of proteins occurs for both pro- and anti-apoptotic responses.

Supplemental Table S1 Primers used for cloning and FISH probe

Primer Name	**Primer sequence (5′ to 3 ′)**
PflE-F	ATATACATGTAAACGGCCTCTCTTATTTC
PflE-R	ATATAAGCTTCCACTTTACGGATAAACATACC
p53-F	ATATGGATCCATGGAGGAGCCGCAGTCAGATCC
p53-R	ATATGAATTCTCAGTCTGAGTCAGGCCCTTCTGTC
Azurin-F	ATATGGATCCACGCCGGGCAGATCCCGCTC
Azurin-R	ATATGAATTCTCACTTCAGGGTCAGGGTGCCCTTCATC
23S rDNA FISH probe with 5′Texas Red	AATCACTTCACCTACGTG

Supplemental Table S2. Mass spectrometry results for identification of Azurin expression (3 biological replicates). Listed are the results detected as AZUR_PSEAE (accession: P00282, species: Pseudomonas aeruginosa). Azurin-negative controls did not have a detectable gel band for mass spectrometry analysis.

Sample ID	Sample Group	# Unique Peptides	Intensity
5	Azurin+	5	1.20E+08
6	Azurin+	5	2.10E+08
7	Azurin+	2	1.40E+07

Supplemental Table S3. Proteomic individual protein snapshot. Shown are the 20 largest by Log2 Fold Change (Log2 FC) magnitude, up- and down- fold changes between each condition pair. Values below the significance threshold are highlighted in red. Please see **Supplemental Information** for complete dataset.

Non-responders relative to Controls

UP Fold

Gene	Accession	Log2 FC	p-value
ALDH1A3	P47895	1.387	0.000606033
HSPB6	O14558	1.35	0.000363856
ETFA	H0YM12	1.195	0.00080317
SDCBP	G5EA09	1.143	2.26E-06
Itgam	G3V8L7	1.13	0.001078139
VPS51	Q9UID3	1.091	0.049194741
Ufc1	Q6BBI8	1.023	0.030357066
Arfgef2	Q7TSU1	1.002	0.034141206
CCDC124	Q96CT7	0.999	0.009064815
Lsm2	Q6MG66	0.996	0.010576147
CTSA	X6R5C5	0.982	0.002856246
H1FX	Q92522	0.972	0.05456802
UQCRH	P07919	0.966	0.022953964
RRP8	O43159	0.959	0.040943669
TUBGCP2	Q9BSJ2-4	0.95	0.02492262
SRP19	P09132	0.947	0.03322118
Emr1	Q5Y4N8	0.928	0.065066637
HNMT	P50135	0.927	0.054959028
Vps53	D3ZPE5	0.922	0.051045151
Cstf2t	M0R6B9	0.911	0.046867016

Responders relative to Controls

UP Fold

Gene	Accession	Log2 FC	p-value
Ppp1r9a	O35867	2.882	9.60E-16
NEGR1	Q7Z3B1	2.799	8.23E-13
Slc6a17	P31662	2.758	2.17E-12
Madd	O08873	2.682	7.51E-13
Rap1gap	F1LV89	2.668	2.47E-09
Caskin1	D3ZE17	2.633	1.20E-15
Ppp1r1b	Q6J4I0	2.603	1.29E-13
Negr1	Q9Z0J8	2.596	3.24E-13
Ppfia3	F1LSE6	2.575	1.19E-13
PTPRD	P23468	2.496	6.11E-08
CALB1	P05937	2.493	2.62E-13
Cep170b	D4A1G8	2.488	6.05E-08
Agap2	Q8CGU4	2.416	7.21E-12
Myef2	D4AEI5	2.373	6.39E-11
Scn2a	P04775	2.349	2.21E-14
Acsl6	A0A0A6YYM0	2.334	2.37E-16
Akap12	Q5QD51	2.327	1.12E-14
Pclo	Q9JKS6	2.324	1.26E-38
Dpp10	Q6Q629	2.322	5.79E-11
Prkce	P09216	2.317	1.20E-10

Responders relative to Non-responders

UP Fold

Gene	Accession	Log2 FC	p-value
Pclo	Q9JKS6	4.549	2.80E-11
Bsn	G3V984	4.36	2.98E-24
Bsn	O88778	4.184	4.34E-27
Gria2	F1LNE4	4.139	8.54E-08
Tnr	A0A096MJE6	3.971	3.38E-14
SYNGAP1	Q96PV0	3.964	8.35E-10
Dmxl2	F1M164	3.932	4.19E-08
Plcb1	P10687	3.857	3.91E-13
Palm	Q920Q0	3.739	2.22E-14
Pde2a	F8WFW5	3.66	2.62E-10
Srcin1	Q9QXY2	3.543	6.77E-20
Ank2	F1LM42	3.529	5.92E-36
Oxr1	Q4V8B0	3.505	3.76E-11
DMXL2	Q8TDJ6-3	3.453	3.49E-12
Camkv	F1LR80	3.45	9.14E-13
SYT1	P21579	3.445	1.50E-35
Synpo	Q9Z327-2	3.432	2.44E-08
Camkv	Q63092	3.426	8.67E-12
Add2	F8WFS9	3.424	9.44E-11
Impact	Q5GFD9	3.413	3.74E-08

Non-responders relative to Controls

DOWN Fold

Gene	Accession	Log2 FC	p-value
Bsn	G3V984	-2.622	1.44E-06
Bsn	O88778	-2.531	6.74E-06
Tnr	A0A096MJE6	-2.218	0.0004623
Plcb1	P10687	-2.123	8.15E-05
Pgrmc1	P70580	-1.97	0.002310608
NCDN	Q9UBB6-3	-1.956	9.16E-05
Hpcal4	P35332	-1.94	0.003098431
Scin	E9PU64	-1.905	0.000154763
Pclo	Q9JKS6	-1.889	0.003141926
Dmxl2	F1M164	-1.851	0.003603893
KRT2	P35908	-1.816	0.000899208
Synpo	Q9Z327	-1.806	0.005110261
Ncdn	O35095	-1.765	0.000144521
Synpo	Q9Z327-2	-1.74	0.008823966
Tmod2	P70566	-1.728	0.003512689
Homer1	Q9Z214	-1.718	0.012052618
Gria2	F1LNE4	-1.714	0.012457946
Camkv	Q63092	-1.704	0.001715614
Add2	F8WFS9	-1.696	0.00342469
L1cam	D3ZPC4	-1.668	0.007714873

Responders relative to Controls

DOWN Fold

Gene	Accession	Log2 FC	p-value
COL6A3	P12111	-4.848	3.75E-28
A1i3	P14046	-4.794	1.85E-14
PRKDC	P78527	-4.561	2.65E-13
Mug1	Q03626	-4.544	1.86E-15
TNC	P24821	-4.449	1.72E-13
ANXA1	P04083	-4.441	9.92E-15
NES	P48681	-4.425	4.68E-12
IQGAP1	P46940	-4.416	4.48E-11
FN1	P02751-15	-4.352	8.74E-11
FLNC	Q14315	-4.272	2.27E-16
AHNAK2	Q8IVF2	-4.256	2.39E-12
MVP	Q14764	-4.115	1.74E-19
TGFBI	Q15582	-4.056	1.83E-11
COL6A1	P12109	-4.035	8.09E-11
Iqgap1	G3V7Q7	-4.019	1.63E-11
KTN1	Q86UP2	-3.971	1.85E-11
A1m	Q63041	-3.955	1.22E-12
Hpx	P20059	-3.933	4.86E-10
CAST	P20810-6	-3.928	8.33E-10
COL6A2	P12110	-3.919	1.38E-10

Responders relative to Non-responders

DOWN Fold

Gene	Accession	Log2 FC	p-value
COL6A3	P12111	-5.025	4.84E-26
PRKDC	P78527	-4.763	3.28E-13
ANXA1	P04083	-4.596	3.56E-13
TGFBI	Q15582	-4.528	7.52E-14
A1i3	P14046	-4.516	8.03E-13
Mug1	Q03626	-4.509	1.69E-11
NES	P48681	-4.473	7.03E-12
FBN1	P35555	-4.452	8.32E-14
AHNAK2	Q8IVF2	-4.451	3.77E-13
IQGAP1	P46940	-4.361	3.20E-13
COL6A1	P12109	-4.313	2.93E-11
TNC	P24821	-4.26	3.84E-13
LGALS1	P09382	-4.26	6.71E-56
MVP	Q14764	-4.206	2.87E-19
FN1	P02751-15	-4.196	4.12E-10
CAST	P20810-6	-4.19	1.24E-11
KTN1	Q86UP2	-4.119	1.03E-11
FAM129B	Q96TA1	-4.086	1.96E-12
PLIN3	O60664	-4.028	1.16E-10
CKAP4	Q07065	-4.002	1.02E-10

Supplemental Table S4. Gene Set Enrichment Analysis (GSEA) snapshot. Shown are the 5 largest positively (red) and negatively (blue) enriched pathways for each condition pair, selected by Normalized Enrichment Score (NES) magnitude. ES: Enrichment score; NOM p-val: nominal p-value given by GSEA; FDR: False Discovery Rate; FWER: Family-wise error rate.

	NAME	SIZE	ES	NES	NOM p-val	FDR q-val	FWER p-val
Non-responders	PROTEIN FOLDING	17	0.6480	2.4384	0.0000	0.0186	0.0090
relative to	ASSOCIATION OF TRIC CCT WITH TARGET PROTEINS DURING BIOSYNTHESIS	10	0.7606	2.3412	0.0000	0.0170	0.0170
Controls	FORMATION OF THE TERNARY COMPLEX AND SUBSEQUENTLY THE 43S COMPLEX	11	0.6838	2.1303	0.0000	0.0788	0.1100
	PEPTIDE CHAIN ELONGATION	33	0.4547	2.1004	0.0000	0.0797	0.1470
	STRUCTURAL CONSTITUENT OF RIBOSOME	27	0.4858	2.0839	0.0000	0.0735	0.1690
	TRANSMISSION OF NERVE IMPULSE	34	-0.6387	-1.6677	0.0000	0.1472	0.6770
	CLATHRIN COATED VESICLE	9	-0.8026	-1.6971	0.0000	0.0985	0.4820
	NEUROTRANSMITTER RELEASE CYCLE	16	-0.7191	-1.7001	0.0021	0.1114	0.4680
	SECOND MESSENGER MEDIATED SIGNALING	14	-0.7356	-1.7007	0.0011	0.1365	0.4610
	SYNAPTIC TRANSMISSION	30	-0.6641	-1.7201	0.0000	0.1147	0.3260
Responders	TCA CYCLE AND RESPIRATORY ELECTRON TRANSPORT	74	0.5741	2.3851	0.0000	0.0000	0.0000
relative to	TRANSMISSION ACROSS CHEMICAL SYNAPSES	60	0.5787	2.2875	0.0000	0.0000	0.0000
Controls	NEURONAL SYSTEM	66	0.5587	2.2337	0.0000	0.0000	0.0000
	RESPIRATORY ELECTRON TRANSPORT ATP SYNTHESIS BY CHEMIOSMOTIC COUPLING AND HEAT PRODUCTION BY UNCOUPLING PROTEINS	49	0.5782	2.2141	0.0000	0.0000	0.0000
	MITOCHONDRION	114	0.4766	2.1351	0.0000	0.0003	0.0020
	NONSENSE MEDIATED DECAY ENHANCED BY THE EXON JUNCTION COMPLEX	35	-0.7143	-2.8738	0.0000	0.0000	0.0000
	PEPTIDE CHAIN ELONGATION	33	-0.7578	-2.8885	0.0000	0.0000	0.0000
	INFLUENZA VIRAL RNA TRANSCRIPTION AND REPLICATION	34	-0.7467	-2.8986	0.0000	0.0000	0.0000
	3 UTR MEDIATED TRANSLATIONAL REGULATION	36	-0.7423	-2.9374	0.0000	0.0000	0.0000

	NAME	SIZE	ES	NES	NOM p-val	FDR q-val	FWER p-val
Responders	NEUROTRANSMITTER RELEASE CYCLE	17	0.7612	2.0635	0.0000	0.0031	0.0040
relative to	ACTIVE TRANSMEMBRANE TRANSPORTER ACTIVITY	30	0.6512	1.9963	0.0000	0.0062	0.0150
Non-responders	NEURONAL SYSTEM	69	0.5640	1.9732	0.0000	0.0065	0.0230
	SYNAPTIC TRANSMISSION	31	0.6445	1.9725	0.0000	0.0049	0.0230
	TCA CYCLE AND RESPIRATORY ELECTRON TRANSPORT	77	0.5515	1.9322	0.0000	0.0071	0.0440
	REACTOME 3 UTR MEDIATED TRANSLATIONAL REGULATION	36	-0.7416	-3.0801	0.0000	0.0000	0.0000
	REACTOME INFLUENZA VIRAL RNA TRANSCRIPTION AND REPLICATION	34	-0.7420	-3.0824	0.0000	0.0000	0.0000
	REACTOME SRP DEPENDENT COTRANSLATIONAL PROTEIN TARGETING TO MEMBRANE	39	-0.7320	-3.0827	0.0000	0.0000	0.0000
	REACTOME INFLUENZA LIFE CYCLE	45	-0.7101	-3.1372	0.0000	0.0000	0.0000
	REACTOME TRANSLATION	52	-0.7248	-3.2511	0.0000	0.0000	0.0000